DRIVERS OF CARBONATE ACCUMULATION IN THE CORDONES FANGLOMERATE

by

Brian Agenbroad

A Thesis Submitted to the Faculty of the

DEPARTMENT OF SOIL WATER AND ENVIRONMENTAL SCIENCE

In Partial Fulfillment of the Requirements

For the Degree of

MASTER OF SCIENCE

In the Graduate College

THE UNIVERSITY OF ARIZONA

2019

THE UNIVERSITY OF ARIZONA
GRADUATE COLLEGE

As members of the Master's Committee, we certify that we have read the thesis prepared by Brian Agenbroad, titled *Drivers of Carbonate Accumulation in the Cordones Fanglomerate, Saddlebrooke, Arizona,* and recommend that it be accepted as fulfilling the dissertation requirement for the Master's Degree.

Craig Rasmussen Date: 4/30/2019

Marcel Schaap Date: 4/30/2019

Michael Crimmins Date: 4/30/2019

Final approval and acceptance of this thesis is contingent upon the candidate's submission of the final copies of the thesis to the Graduate College.

I hereby certify that I have read this thesis prepared under my direction and recommend that it be accepted as fulfilling the Master's requirement.

Craig Rasmussen Date: 4/30/2019
Master's Thesis Committee Chair
Soil, Water and Environmental Science

TABLE OF CONTENTS

ABSTRACT

The accumulation of pedogenic carbonates is important to understanding carbon cycling, to include carbon sequestration, in arid and semi-arid regions. Carbonate accumulation in southern Arizona displays significant spatial variation, particularly in alluvial deposits that dominate basins in the region. Improved understanding of the controls on pedogenic carbonate accumulation is needed. Here it is hypothesized that carbonate accumulation in alluvial fans is controlled significantly by parent material composition. To address this hypothesis, samples were taken from a chronosequence consisting of multiple buried horizons and carbonate accumulations. Parent materials include calcareous and non-calcareous meta-sedimentary rocks, diabase, granites and schist. Measurements included carbonate concentration using a traditional method of hydrochloric acid digestion. This was compared to results generated with an infrared spectral curves for calcium carbonate concentration. Bulk elemental content was obtained via X-ray fluorescence analysis for quantification of immobile element accumulation. Pedogenic iron contents extracted by both sodium dithionite and ammonium oxalate, were taken as indicators for changes in weathering. Results indicate that a mix of eolian material and calcareous rocks are the dominant sources of carbonate accumulations.

INTRODUCTION

With atmospheric carbon continuing to be a growing concern, understanding natural carbon sinks remains a worthy focus of research. A very effective sink, in terms of longevity, is the production of calcium carbonate carried out by marine organisms which becomes sequestered in deep sea sediments. Lithification of marine sediments results in the long term sequestration of carbon in the form of carbonate minerals. This sequestration continues in the terrestrial sphere where ancient sea floors are represented by carbonate rocks. These rocks, however, are subject to weathering reactions on the surface that utilize atmospheric carbon. For example, limestone weathering utilizes one mole of carbon dioxide

$$CaCO_3+CO_2+H_2O \leftrightarrow Ca^{2+} + 2\ HCO_3 \qquad \{Eq.\ 1\}$$

However the reverse occurs when calcium carbonate is precipitated. One mol of CO_2 is released (Liu and Zhao, 2000). Though a mole of CO_2 is released, the $CaCO_3$ still represents one mole of carbon sequestered in a potentially long lasting form.

When precipitated, carbonates accumulate in soils forming a secondary pool of inorganic carbon. Additionally, free ions of calcium, magnesium and other mineral forming elements are produced from the weathering of primary minerals. For example, anorthite and diopside are of sources of calcium; enstatite and forsterite are sources of magnesium. These can become part of

the soil solution via direct weathering of igneous rocks and combine with bicarbonate molecules to precipitate secondary carbonate minerals. Some general formulas describing $CaCO_3$ precipitation are as follows.

$CO_2 + H_2O \leftrightarrow H_2CO_3$ {Eq. 2}

$H_2CO_3 \leftrightarrow HCO_3 + H^+$ pK=6.4 {Eq. 3}

$HCO_3 \leftrightarrow CO_3^{2-} + H^+$ pK=10.3 {Eq. 4}

$$K_H = \frac{(H_2CO_3)}{P_{CO_2}} = 10^{-1.5}$$ {Eq. 5}

$Ca^{2+} + 2HCO_3 \leftrightarrow CaCO_3 + H_2O + CO_2$ {Eq. 6}

Equations 2-4 describe the dissolution of carbon dioxide in water and the production of the bicarbonate ion followed by the carbonate ion. Equation 5 describes the amount of carbon dioxide available in soil based on Henry's law. Equation 6 describes the precipitation of calcium carbonate.

In soils, P_{CO2} is generally higher in at depths of 30-50 cm due to the presence of roots and the associated presence of heterotrophic microbes (Turk et al. 2012). Soil solution here will be more acidic disallowing the precipitation of carbonate minerals. As constituents leach downwards towards a zone of lower P_{CO2}, conditions become more favorable for carbonate precipitation (Turk et al. 2012). Precipitation of solutes occurs more readily in semi-arid and arid regions, as there is

generally not enough water to leach solutes completely out of the soils (Brockheim 2014).

Estimates of carbon in soils range from 1500 to 2000 Pg of organic carbon and 930 to 1738 Pg of soil inorganic carbon (SIC). Soil carbon represents approximately two thirds of the terrestrial budget and soil inorganic carbon pools represent half of that by some estimates that (Rasmussen 2006). SIC typically exists in soils in the form of carbonate minerals with calcite, magnesite and natrite being the most common examples (Turk et al. 2012). Of these $CaCO_3$ is the dominant form (Nash 2011) and is the focus going forward. $CaCO_3$ precipitates at pH levels between 7.2 (Turk et al. 2012) and 9.0 (Nash 2011).

Further understanding of the effectiveness of developing soils as carbon sinks is crucial. To illustrate, if the development of carbonate enriched soil horizons were to be driven solely by the dissolution of limestone and re-precipitation of calcium carbonate, there would be no net gain in carbon sequestration, there would be only a change in sink. Likewise, without other factors, it appears that weathering of carbonate rocks into fines represents only a transfer of carbon from one sink to another with no increased sequestration into the new sink. However, the difference between the dissolution of carbonate rocks and carbonate fines becomes a question of rate. Fines, such as eolian transported carbonates, will more readily

dissolve representing a relatively quick (compared to the weathering of rocks) draw down of CO_2 until the carbonates again precipitate in the soil. Precipitation of carbonates in the soil introduces CO_2 into the soil air which may or may not return to the atmosphere, depending on other soil factors. With an addition of free ions to the system, however, there is potential for an actual increase of carbon sequestered in mineral form in the soil.

The latter scenario is worth investigating to gain understanding of whether soil carbonates are being quickly dissolved and precipitated or if the carbonates are more commonly derived from the slower weathering of rock. The possibility of free calcium contribution from the weathering of primary minerals is also worthy of investigation given the existence of a missing terrestrial carbon sink. An estimated 0.4 to 4 Gt C/yr is "missing" from the global carbon budget and is thought to exist in an unknown sink (Gifford, 1994). Previous hypotheses, such as a nitrogen driven increase on the primary production of northern forests, have fallen away (Schindler, 1999) leaving the possibility that soil inorganic carbon may play a role in this missing sink (Mi et al. 2008). The limiting factor in question here is the source of free ions used in the formation of carbonate minerals in the terrestrial sphere. Are they derived solely from reworked, carbonate, sedimentary rocks,

or is there a significant amount of free ions supplied by the weathering of igneous rocks and/or the atmosphere?

It is possible to gain better understanding of the impact of SIC on the global carbon cycle given accumulations of SIC that occurred over known spans of time and during known climate conditions. In the arid southwest U.S. accumulations of SIC are common in sediments of Pleistocene age (Machette 1985). The Pleistocene, spanning a period from 11.7 to 2580 ka (Walker et al. 2013) was characterized by repeated changes in climate associated with oscillations of glacial and interglacial conditions in the northern hemisphere (Ehlers et al. 2018). Analysis of SIC accumulations in Pleistocene aged soils can yield insight into the rate at which such accumulations develop and contribute to terrestrial carbon cycling.

Calcic and Petro-calcic Horizons

Here focus is on soils where soil inorganic carbon, especially in the form of calcium carbonate (though magnesium carbonate can also be common), that has accumulated into calcic and petro-calcic horizons in arid regions. Arid systems (defined here as areas occupied by aridisols) comprise approximately 12% of the global land surface and account for approximately 20% of the global pool of SIC (Rasmussen 2006). Due to low precipitation, carbonates in arid systems form discrete masses

and cemented sediments known taxonomically as calcic for non-cemented horizons and petrocalcic for cemented horizons In the continental United States, approximately 13.8% (~ 1,061,090 km^2) of the total soil area meets the requirements to be considered calcic or petro-calcic (Brockheim 2014). A study of regions undergoing desertification in China (Feng et al. 2001) found approximately 14.91 Pg of SIC stored in the top meter of those soils. The application of the term "desertification" excluded regions that had long been arid and those which could be expected to recover from drought conditions. Given the restriction of the term, it is very likely that the total amount of carbon stored in China's soils is much higher. These figures show that soil organic carbon in arid regions is a significant terrestrial sink for carbon. The processes under which these carbonates form are important to understand.

To be classified as calcic, a horizon must be ≥ 15 cm thick, be comprised of 5 – 15% $CaCO_3$ (depending on clay content), have 5% more $CaCO_3$ than the underlying horizon and lack cementation or induration (Soil Survey Staff, 2010). Petro-calcic horizons must be ≥ 10 cm thick (≥ 1 cm as a laminar cap over bedrock), display cementation or induration and have lateral continuity of at least 10 cm (Soil Survey Staff, 2010). Roughly 94% of soils with calcic and/or petrocalcic horizons lie within mesic, frigid/cryic and thermic temperature regimes (Brockheim, 2014).

Here mesic is defined as mean annual soil temperatures of 8° C to 15° C at 50 cm depth with a >5° C difference between summer and winter values (Buol et al. 2003, Schaetzl and Anderson, 2005).

Frigid and cryic are defined as temperatures ranging from 0° C and 8° C, at 50 cm depth, with a >5° C difference in summer and winter values. The frigid regime has warm summer temperatures whereas the cryic has cold summer temperatures. Thermic is defined as a mean annual soil temperature of more than 15° C but less than 22° C and a greater than 5° C difference between seasons at 50 cm depth. (Schaetzl and Anderson 2005).

The most represented moisture regimes are aridic/torric and ustic (44% and 26% respectively). Aridic/torric are defined with the same attributes: a lack of moisture for at least half of time during which the soil, at 50 cm depth, is >5° C and their soil is never moist for longer than 90 consecutive days when the temperature is at 8° C at 50 cm depth (Schaetzl and Anderson 2005). Ustic is defined as a moisture regime falling between aridic and udic where udic is defined as dryness that never lasts 60 consecutive days in the three months following the summer solstice and is never dry for as long as 90 consecutive days for the rest of the year (Schaetzl and Anderson 2005). In the U.S. petrocalcic horizons are found mostly in the basin and range province spanning western Texas, New Mexico, California and Arizona with some being located in Nevada and Utah. Calcic

horizons are found abundantly in the same regions but can also occur in specific sites in locations such as North Dakota, South Dakota, southern Idaho, Colorado, Utah and western Minnesota (Brockheim, 2014) (fig. 1).

Calcic and petrocalcic horizons are found in soils primarily from alluvium (55% for calcic and 66% calcareous alluvium for petrocalcic). Calcic horizons may also be found in soils from derived from colluvium and residuum (11% and 8% respectively). Calcareous eolian material is attributed to the development of 33% of petrocalcic horizons (Bockheim, 2014). Vegetation that dominates soils with calcic and petrocalcic horizons includes short, mid and tall grass prairie, as well as desert scrub (Bockheim 2014).

Development of Calcic and Petrocalcic Horizons

The development of petrocalcic and calcic horizons depends largely on a lack of soil moisture that limits the loss of dissolved components to leaching and allows for the accumulation of soluble salts in subsurface horizons. The mean annual precipitation associated with petrocalcic horizons is 392 mm/yr with a mean annual temperature of 17.6 °C (Bockheim 2014). Some research relates the depth to carbonate accumulation to mean annual precipitation (McFadden and Tinsley, 1985 ; Marion, 1989) and correlations may make carbonate accumulation depth a useful

proxy for past climate (Retallack, 2005). McFadden and Tinsley (1985) introduced a model to project the distribution of carbonate accumulation in a soil under known parameters. Their model breaks a soil profile down into compartments each with its own values of texture, water-holding content, bulk density, mineral composition, soil-air pC02, solution ionic strength, and temperature. Their model projects distributions of carbonate at varying depths that is driven by a leaching index, defined as the effective annual soil water in a 1 cm^2 column. Soils in arid and hyperthermic settings were projected to have carbonate accumulations at depths of about 0-5 cm, whereas carbonate accumulations in xeric, thermic regimes could occur as deep as 300 cm (McFadden and Tinsley 1985). The model results were compared to soils in the Mohave Desert of California. The models reflected decent similarity with the observed soils in terms of depth to carbonate. McFadden and Tinsley's (1985) model also projected bimodal distribution of carbonates over the climatic transition between the last glacial maximum and the Holocene epoch. However, Royer (1999) produced a regression analysis that resulted in poor correlation between depth to carbonate accumulation and precipitation.

Shankar and Achyuthan (2007) report that petrocalcic horizons reside at greater depth in high relief deposits. Since groundwater can move upward to deposit carbonate material,

relief and level of groundwater become important factors. However, Machette (1985) notes that the typical grain sizes of sediments dominating the arid US southwest are generally too large to provide the potential for the capillary rise. Other factors influencing the accumulation of carbonates in soils are the presence of microbes and plant roots. It has been shown that fungi and bacteria both precipitate calcite when grown in calcium enriched media (Monger et al. 1991). Biogenic structures such as calcified root cells and filaments in calcic soils in India (Shankar and Achyuthan, 2007) provide evidence of the influence of plant life.

The resulting stages of carbonate development can be both an indication of age and climate (Birkeland 1999) (fig. 2). Carbonate stages are classified approximately as follows: Stage 1- thin coatings of carbonates on grains (pebbles and gravels); Stage 2- carbonate nodules separated by low carbonate material; Stage 3- at least 90% of the interstitial spaces between grains is filled by carbonate nodules and/or filling; Stage 4- laminations form above the carbonate filled horizon. Machette (1985) added two more stages: Stage 5- both laminate and pisoliths form above the carbonate filled horizon; Stage 6- pisoliths, brecciation and re-cementation are present. The general trend of carbonate accumulation through time is a transition from Stage 1 to higher stages with increasing soil

age. The change in carbonate stage may be offset by climate where, given enough precipitation, (roughly > 25.0 cm) carbonates of stages 3 and 4 can occur at ages typical of carbonates at stages 5 and 6. Conversely, given high enough temperature (and despite precipitation > 30 cm) carbonates of stages 4 and 5 can be as young as is typical for stage 3 carbonates. The general progression of greater carbonate stage with greater age is echoed in both clay accumulations and soil redness ratings (Birkeland 1999). Clays, though also affected by climate driven weathering, tend to show greater accumulations with age. Likewise, redness progresses with age. Though neither factor is useful as a relative age indicator against the others, taken together a rough age estimation can be made for soils with carbonate accumulations.

Machette (1985) also developed a model for carbonate accumulation rates. Again he noted that, in general, greater development (carbonate concentration and thickness) of carbonate accumulations relates to greater age. Machette (1985) found that carbonate accumulation rates are driven primarily by the influx of calcium and the amount of precipitation (fig. 3). Therefore, estimates of Ca influx and precipitation amounts can be used to estimate the soil age, based on amount of secondary carbonate present in a 1 cm^2 column. However this model is not useful for

soils with calcareous parent material (Machette 1985).

Origin of Carbonates

Currently, debate exists concerning the origin of the materials necessary for carbonates to accumulate. The question primarily involves atmospheric calcium (dust and rain) as a primary source (Lattman 1973; Machette 1985; Chadwick and Davis 1990; Van der Hoven and Quade 2002) or in-situ parent material as a primary source (Sobecki and Wilding 1983; Rabenhorst et al. 1984, 1986; Boettinger and Southard 1991). Sources of atmospheric calcium are varied, though dust particles are again thought to be a common source (Junge and Werby 1958; Schmitt and Stille 2005). A study of calcium isotopic ratios from various sites around the globe concluded that carbonates are a common origin for calcium in rain water (Meszaros 1966) however, data from a water shed in the Vosges Mountains in France showed a mix of calcium from carbonate dust and calcium from leaf excretions (Schmitt and Stille 2004). The values utilized were $\delta^{44/40}Ca$ measured by mass spectrometry. This method allowed sea spray to be ruled out by showing that proximity to the Atlantic resulted in negligible difference. The ratios also ruled out industrial inputs, which showed negligible fractionation of the calcium (Schmitt and Stille 2005). The Vosges Mountain data allowed a rough estimate of 70% for calcium originated from atmospheric

contributions leaving roughly 30% to originate from uptake and excretion by trees. This allows for a potential mechanism for calcium to be aerosolized from droplets excreting from tree leaves. Seasonal shifts in the calcium isotopic ratios in the local streams support the Vosges data. During high discharge periods, the stream water is enriched in Ca^{44} because the trees preferentially take up Ca^{40} during the growing season. Conversely, they are depleted in the heavier isotope during the off season (Schmitt and Stille 2005).

In coastal regions, sea spray can be a source of numerous soil cations including calcium (Art et al. 1974). An analysis of strontium ratios from the Pahala tephra, located on the Island of Hawaii, suggested that sea spray was a significant contributor to the carbonate accumulation within the tephra (Whipkey et al. 2000). Possible sources of strontium at this location include sea spray, the parent material, eolian material and rain water. The parent material Sr87/Sr86 was ~0.7035, the rainwater/sea-spray was ~0.7092 and the eolian material was ~0.72. Additionally it was reported that dust was not a major contributor to the carbonate accumulation in older, nearby Hawaiian soils and dust is not likely to be a major contributor to the younger Pahala site. Rain water is reportedly very difficult to separate from sea spray since both derive from the ocean, however, the Pahala site is classified as semi-arid

rendering rainwater an unlikely source. The labile soil reservoir had Sr87/Sr86 of ~0.70622 – 0.70825. These results suggested that 48-83% of the strontium in the labile reservoir derived from sea spray. Using strontium as a proxy for calcium, this suggests that approximately 43-67% of the soil Ca was also derived from sea-spray (Whipkey et al. 2000).

To be thorough, cosmic dust is also considered. The presence of cosmic dust is determined by Ir and Ni values which are enriched in chondritic material by 10^4 and 10^2 respectively. These values also rule out volcanism as being the primary source (LaViolette 1985). The ice core analyzed by LaViolette (1985) was taken from Camp Century in Greenland and was selected to avoid the influence of basal ice deformation on the data. The outer layers of the core were melted away with purified DI water to remove any contamination introduced by drilling chemicals. LiViolette (1985) reports a global cosmic dust deposition rate of 1 E^5 to7 E^5 tons (0.91 to 0.64 Tg) a year and a 0.5 E^7-3 E^7 (4.50 to 27.22 Tg) during the last ice age. This increase is interpreted to be due to an increased introduction of cosmic material into our solar system during the late Pleistocene. LaViolette (1985) notes that ice accumulation rates were assumed constant, which introduces error, and that fluctuations in Ir and Ni concentrations of cosmic dust cannot be accounted for. Building on this, an analysis of interstellar dust composition

from samples taken by the Cassini spacecraft near Saturn is also considered (Altobelli et al. 2016). The cosmic dust analyzer aboard the Cassini collected ten years of data. Analysis of this data by Altobelli et al. (2016) concluded that the composition of current interstellar dust closely matched that of C1 chondrite elemental abundances. Anders and Ebihara (1982) reported an updated table of C1 chondrite elemental abundances which gives a solar system abundance of calcium of approximately 0.98%. This is close to the composition of the Orgueil chondrite reported in the same paper as approximately 0.9% (Anders and Ebihara, 1982). As a preliminary estimate of the high end, this would be approximately 0.24 Tg of calcium added to Earth per year during the late Pleistocene. Even assuming this added calcium to be in the form of free calcium (the mineral forms were not reported) this high end estimate represents a very small amount relative to the 504 Tg (Maybeck, 1987) estimated to be derived from rocks.

Machette (1985) suggests atmospheric calcium as the primary source, due to the weathering resistance of igneous rocks, formation of calcic horizons within non-calcareous sediments, the presence of local parent materials that provide calcareous dust, and the calcium content of rain water in the southwestern United States. The calcium content of the rain water in the region can be greater than 5 mg per liter (Junge and Werby

1958), though the highest concentrations were reported over the Southwest region and were attributed to atmospheric dust. Dust fall in the region is estimated to supply 0.2 grams of $CaCO_3$ per cubic centimeter per 1000 years (Machette 1985). Comparisons of carbonate accumulation in soils with regards to their position in relation to dust sources has shown that those soils downwind of dust sources tend to have greater accumulation of carbonates (Lattman 1973; Chadwick and Davis, 1990). It should be noted that Lattman (1973) reports exceptions to fans containing limestones and/or dolomites as parent material. Vanderhoven and Quade (2002) employed strontium isotopic ratios as tracers of calcium to show that carbonates accumulating in a volcanic field near Grants, NM were primarily attributable to eolian deposition of carbonates from marine deposits. One cinder deposit aside, strontium ratios of the labile fractions of "A" horizons in this locale had values in common with local sources of carbonate rock. Strontium ratios of the accumulating carbonates plotted much closer to the ratios of the labile fraction than they did to the basaltic parent materials indicating that accumulating carbonate was likely derived from eolian material (Vanderhoven and Quade 2002).

In contrast, Sobecki and Wilding (1983), in a study of soils within a coastal prairie in Texas, ruled out both the weathering of silicate rocks and atmospheric calcium as primary

causes of carbonate accumulation. Calcium bearing silicate rocks were not abundant enough to have account for the amount of accumulated carbonates. Sea spray was ruled out as a source given measured salt concentrations as it would require too much time to accumulate the calcium at the given rate of deposition, to account for the amount of carbonate present. Additionally a highly impermeable layer of clay material underlying the soils restricted calcium carried upwards by deeper ground water sources, leaving calcium bearing, allogenic, parent sediments within the soils as the most likely source of carbonate accumulation. (Sobecki and Wilding, 1983).

Rabenhorst and Wilding (1984) found evidence for limited downward translocation of material in soils forming from limestones in western Texas. The evidence included a low amount of non-carbonate residues in the petrocalcic horizons that displayed differing mineralogy, size and trace elements than that of the overlying soil horizons. Fluorite, a labile mineral was found in some of the petrocalcic horizons. Labile minerals would likely not be present in a soil previously leached of carbonates. These findings suggest that the source of the carbonate accumulation could not have been brought into a previously carbonate depleted soil and deposited on the surface. Morphological characteristics of the carbonates, which indicated alteration of lithogenic carbonate crystals, suggested in-situ

alteration of the limestone parent material (Rabenhorst and Wilding, 1986).

Boettinger and Southard (1991) reported the accumulation of secondary carbonates adjacent to carbonate free soils on the same geomorphic surface. The carbonate accumulations lie under duripans and have developed on, and within, well degraded saprolites of calcareous granitic rock. The carbonate free soils also lie under duripans but exist over less degraded and carbonate free saprolites. Given the uneven distribution of the carbonate rich pedons, it is unlikely that eolian material is the primary source of the carbonate material in these soils. Though the source of the carbonates cannot be stated with surety, the presence of carbonate accumulation in the well degraded saprolites suggests calcium derived from the weathering of plagioclase (Boettinger and Southard 1991)

In the cases presented above, all but one reported carbonate accumulation for which the requisite materials were derived from pre-existing carbonate sources in the form of eolian dust or in-situ carbonate rocks and/or sediments. Carbonates in these systems are dissolved and re-precipitated with very little free calcium added to the system from the weathering of calcium bearing, igneous rocks.

Maybeck (1987) conducted a study of exorheic (flowing to the ocean) French rivers to obtain a global estimations of

dissolved load in rivers and the percentages contributed by various rock types. Remote rivers were selected to reduce contamination of the data by pollution and watersheds were selected to limit contributing rock types. Results were compared to similar studies from other regions and corrected for atmospheric contributions. The total amount of calcium released from chemical weathering reported was approximately 504 Tg/yr. Of this, granitic rock was estimated to contribute 0.6% or 3 Tg/yr, volcanic rock 1.8% or 9 Tg/yr, metamorphic rocks 4.8% or 24.2 Tg/yr, and sedimentary rocks (to include gypsum and rock salt) 91.8% or 462.7 Tg/yr. Carbonate rocks contributed the greatest amount of calcium to dissolved load, representing 60.4% or 303.4 Tg/yr (Maybeck 1987). It was noted by Maybeck (1987) that differing temperatures can have a notable impact on chemical weathering rates. Rates in arid climates are likely much lower due to the greatly reduced moisture. Given the similar values between different regional studies reported by Maybeck, it is reasonable to conclude that contributions of free calcium from igneous rocks in arid regions is at least similar in terms of proportion. It is also reasonable to suspect that non-exorheic streams contain similar proportions and contribute to the deposition of material that can later be further distributed by eolian processes, resulting in the deposition of fines, that can be easily dissolved and re-precipitated at depth

in soils.

Uncertainties concerning the sources of atmospheric calcium, as well as the missing fraction of the carbon budget, invite further research. The excretion of calcium taken up by desert plants could be an important addition to atmospheric calcium in arid climates. For instance, it was reported by Tatarko (1980) that creosote bush grew more abundantly on soils enriched in $CaCO_3$. Climatic shifts over the Pleistocene introduced cyclic wet and dry periods, as well as drastic changes in atmospheric circulation, that had significant effect on rock weathering, eolian deposition and biological activity. Further research focusing on the accumulation of carbonates under known climatic shifts could potentially shed light on the contributions of numerous factors involved in soil carbonate accumulation, especially concerning the question of eolian input vs the weathering of parent material.

Here we focus on soil carbonate accumulations in Southern Arizona to determine the primary source of carbonate from which the accumulations are derived. A key question is: Are the accumulations primarily due to eolian transport and deposition, or are they primarily due to the weathering of local, carbonate rocks? Secondarily, focus is placed on how changes in climate over the Pleistocene may have impacted the accumulation of soil

carbonate.

MATERIALS AND METHODS

Study Area and Geologic History

To better understand the influence of carbonate redistribution consideration is given to a remnant alluvial fan located approximately a mile northwest of Saddlebrooke, AZ (UTM: 12 S 511954.90 m E 3602702.26 m N ; fig. 4). The site was selected due to features, exposed in a road cut, that suggest a record of multiple episodes of sedimentation and soil development. The fan was formerly fed by a stream flowing out of the Canada Del Oro HUC-12 sub-watershed (Stroud Water Research 2018) in the Santa Catalina Mountains. Carbonate accumulation and lithologic discontinuities observable in the field suggest at least two buried sequences (fig. 5). The parent materials comprising the fan can be characterized as mixed alluvium. A rough estimate of specific materials available to the fan can be gained by overlying the USGS Watershed delineation with current geologic maps (fig. 6). Approximately 60 percent (by map area) of the outcropping rock in the watershed is granitic rock. The remaining 40 percent is divided among various metamorphic and sedimentary rocks which include two sources of carbonate material, the Mescal limestone and the Abrigo shale. The fan

itself has been named a geologic unit called the Cordones Fanglomerate (Spencer 2000).

The fan covers approximately 36 km^2 and has been heavily incised with a drainage density of approximately 0.55. The southwestern edge of the fan is characterized by a prominent erosion face (fig. 4) that indicates that the current path of the Canada Del Oro wash is younger than the fan. Previous studies date the fan sediments as Pleistocene–Pliocene (Spencer et al. 2000), and the work of McFadden (1981) dates the soil on the fan surface from mid to early Pleistocene. These dates were supported by morphological features and soil development such as a clay enriched argillic horizon, very red coloration, and stage 4 carbonate accumulation. The surface soil at the sample location was classified as an Ustalfic Petrocalcid. The argillic horizon extends from about 18 cm to 35 cm, has a hue of 2.5 YR and contains about 60% clay. It rests on top of a cemented, laminar cap that is 2-5 cm thick. Below the laminar cap the profile loses its redness, lightens in color, and undergoes changes in lithologic character. The lighter color is due to accumulations of pedogenic carbonate (determined by effervescence). There is a band of redder material at approximately 2.35 m (referred to from this point on as the red band) that is approximately 10-12 cm thick. Underlying the red band are two calcic horizons separated by a band of lower

carbonate accumulation at approximately 3 meters of depth. The profile overlies a basal gravel. The grains in this layer are angular to sub angular, silt to cobble in size, with minor carbonate rinds present on some clasts.

The fan surface likely represents a relict surface, deposited prior to numerous cut and fill sequences associated with Pleistocene climate fluctuation. Based on estimated ages of the Cordones surface, the deposition and subsequent incision of the fan likely correlates to Quaternary fill observed in other locations in southern Arizona such as the Aravaipa Basin, Safford Basin and Sonoita Basin. Jungers and Heimsath (2018:2015) report burial ages (Al^{26} and Be^{10}) on similar surfaces in the Aravaipa and Safford basins at ~1.8 to 3 Ma. The depositional period here is attributed to a more precipitation prone climate between 3.5 Ma to 2 Ma which lead to increased erosion rates in the surrounding mountains. Menges and McFadden (1981) report Miocene-Pliocene aged basin fill (based on magnetostratigraphy) topped with Pleistocene alluvial fans in the Sonoita Basin. The Pleistocene deposits are termed the Martinez formation. They are characterized by clay rich diamictons (poorly sorted, sand to boulder grain sizes) which separates them from the older fill they rest on. The magnetostratigraphy of the underlying basin fill established a 3-2 Ma maximum age for the Martinez surface. A minimum age of 1

Ma is reported due to degree of soil development, within the Martinez fans, consisting of distinct argillic and calcic/petrocalcic horizons (Menges and McFadden 1981). These observations agree with the general, regional observations of Morrison (1991) who reported Pleistocene depositional surfaces containing well developed soils expressing horizons of clay and carbonate accumulation. The Cordones surface fits the profile of these regional, Pleistocene surfaces in age estimation, lithological character, and degree of soil development. For these reasons, Menges and McFadden (1981) associated the Martinez Surface with the Cordones surface putting its age between 1-2 Ma.

The geologic history of the parent rocks that sourced the Cordones Fanglomerate begins with the Pinal Schist. The schist has been dated to approximately 1.69 to 1.7 Ga (Livingston 1969 ; Silver 1978). This time frame suggests that the original sediments were deposited in a marine environment given paleogeographic reconstruction (Blakey 2011). The later metamorphism is attributed to two different causes, sediments being deposited in rifting basin leading to high temperature/low pressure metamorphism associated with rifting (Condie and DeMalas 1985 ; Wickham and Oxburgh 1985). The geochemical data, however, is also indicative of collisional regimes (Condie and DeMalas 1985). This is followed by the intrusion resulting in

the Oracle granite which has been dated to approximately 1.45 Ga (Damon et al. 1962 ; Silver 1978). This intrusion is older, relatively speaking, than the Apache Group due to the presence of Oracle Granite clasts within the basal, Scanlon Conglomerate.

Deposition of the Apache Group, which includes the Pioneer shale, Dripping Springs quartzite and Mescal limestone, is dated between 1.45 Ga (the date of the underlying oracle Granite. Damon et al. 1962 ; Silver 1978) and 1.1 Ga based on the date of diabase sills that intrude into the entire group (Livingston and Damon 1968). Fletcher et al. (2004) give dates, derived from detrital muscovites of 1.33 Ga for the Pioneer Shale and 1.2-1.1 Ga from the Dripping Springs quartzite. The Apache group lies unconformably on both the Oracle granite and the Pinal schist (Middleton and Trujillo 1984) indicating a depositional hiatus. The basal unit of the Apache group, the Scanlon Conglomerate, displays cross-bedded facies interpreted by Middleton and Trujillo (1984)as deposition associated with alluvial fans and braided stream systems thus establishing a terrestrial depositional setting for this unit. Channels within the Pioneer Shale filled with Barnes conglomerate and the overlying arkose member of the Dripping Springs quartzite lacks tuffaceous materials. This is taken by Shride (1967) as suggestive of a possible hiatus in deposition between the Pioneer shale and Dripping Springs Quartzite. Stratified and crossbedded tabula

within the arkose member suggests deposition in a shallow sea subjecting the sediments to wave action (Shride 1967). Ripples, mudcracks, thin irregular bedding and scour-fill structures are suggestive of tidal flats and very shallow water, in effect, the margin of transgressing/regressing sea (Shride 1967). The Mescal limestone lies unconformably on top the of Dripping Strings quartzite, as evidenced by an undefined sandstone unit separating the quartzite and the limestone in more northerly parts of Arizona. The limestone represents a marine depositional environment with potentially low circulation and a stable sea floor, evidenced by an accumulation of halite, dolomite and the growth of stromatolites in biostromes rather than bioherms (Shride 1967).

The Bolsa Quartzite lies unconformably on the Mescal limestone. This is evidenced by a lack of intruding diabase and a disconformity on basalt flows topping the Mescal limestone in some areas of the state (Heindyl and McClaymons 1964). Brachiopods fossils and preserved worm burrows indicate a near shore, depositional environment. These sediments were later buried by the sediments of the Abrigo formation which lies conformably above (Heindyl and McClaymons 1964).

The Abrigo formation represents offshore, transition and shore-face depositional environments dominated by wave and storm activity in the Sauk sea (Labaj and Pratt 2016). The formation

includes varying proportions of siliclastic and carbonate sedimentation which is interpreted to result from a dynamic flux of material from the land which periodically shut of carbonate production. The facies outcropping in the Santa Catalina Mountains represents one of the more calcareous examples (Labaj and Pratt 2016).

A great deal of depositional history is missing between the Abrigo shale and the tertiary igneous rocks present in the watershed. The Rice Peak porphyry is an intrusion associated with the Laramide Orogeny (70 - 40 ma) while the Catalina granite is a later intrusion (25 ma) (Fornash et al. 2013). These intrusions are associated with the onset of regional extension and associated basin sedimentation. The exhumation of the Catalina core complex began in the late Miocene based upon the dating of mylonitic fabrics, and continued into the Pliocene, given the tilted orientation of Tertiary conglomerate as well as its inclusion of the mylonitic clasts (Fornash et al. 2013). The faulting in the area is also associated with the Late Miocene extension and continued into the Pliocene, with the last movement of the Pirate fault reported to have likely occurred approximately 6 Ma (Davis et al. 2004). Following the deposition of the Tertiary conglomerate, and Miocene-Pliocene basin fill, the Cordones Fanglomerate was deposited.

Unit Descriptions

The following unit descriptions are taken from Spencer et al. (2000) with additional information cited in the descriptions. Map symbols used here differ from the Spencer et al. (2000) paper and are taken from a geologic map of Arizona produced by Richard et al. (2000). For this reason, some unit descriptions are condensed to match the map symbols utilized by Richard et al. (2000). The map symbols utilized by Richard et al. (2000) encompass wider examples of rock found throughout the state of Arizona. Only those rocks pertinent to the study are described here.

Proterozoic Rocks (~ 2.5 Ga to 542 Ma)

- The Pinal Schist (map unit Xms) is an Early Proterozoic (Condie and Demalas 1984; Silver 1978) to Middle Proterozoic, pale gray to gray schist and psammitic schist with sufficient metamorphosis to cause finer grain stones to display significant phyllosilicate development with cleavage parallel to the preferred orientation of the phyllosilicates. Quartz veins are abundant, especially in finer grain stones.
- The Oracle Granite (map unit Yg) is a Middle Proterozoic, coarse grained, porphyritic, biotite granite representing

the intrusion of a felsic magma. The granite also displays mylonitic fabrics and biotite displaying severe argon loss in locations adjacent to the Mogul fault that is associated with basin and range orogenesis (Damon et al. 1962).

- The Apache Group (~ 1.33 Ga to 1.1 Ga; map unit Ys)
  - The Pioneer formation (sometimes called the Pioneer Shale) is a generally massive grey to lavender argillite, metasiltstone and very fine grained, thin to medium bedded metasandstone. The formation includes a basal conglomerate (called the Scanlon Conglomerate) that consists of angular to sub-rounded pebbles and cobbles. Clasts are bull quartz, fragments from the Pinal schist and fragments from the Oracle granite.
  - The Dripping Springs Quartzite is thin to medium bedded, fine to medium grained quartzite with silty laminations. Locally it tends to be pale grey, thick bedded and massive. This unit includes a clast supported basal conglomerate (called the Barnes Conglomerate) up to 10 m thick that consist of sub-rounded to well-rounded clasts of white quartz, red jasper and quartzite up to 20 cm in diameter. The quartzite can be roughly divided into a lower arkose member and an upper siltstone member (Shride 1967)

  - The Mescal Limestone is laminated to thin bed, and light to medium gray to tannish gray. It contains gray, 1 to 30 cm thick chert beds and siliceous thin beds, lenses and nodules that form tan to brown rib-like protrusions between recess forming carbonate layers. Rocks of this unit tend to locally part along silty layers to form slabs.

- The Sierra Ancha Diabase (map unit Ys) is dark gray, dark greenish gray and grayish black rock existing in sills and dykes showing typical, sub-ophitic, dibasic texture.

Paleozoic Rocks (map unit MЄ)

The Abrigo shale and Bolsa quartzite are both found in this watershed however their position in relation to each other is not consistent (Spencer et al. 2000). The northern most exposures the lithologies are mixed and difficult to stratify. Within more southern exposures the Bolsa quartzite is over lain with the Abrigo shale (Spencer et al. 2000). Heindyl and McClaymons (1964) report that the Abrigo Shale underlies the Bolsa Quartzite in other parts of the state. Here the stratigraphic findings of Spencer et al. (2000) are treated as specific to the study area.

- The Bolsa Quartzite is a Cambrian, fine to coarse grained, thin to thick bedded resistant quartzite composed of 95% quartz and feldspars. Vitreous, light gray to whitish gray crossbeds are accentuated by dark colored laminations rich in magnetite in areas where Proterozoic diabase was exposed during Cambrian deposition. Elsewhere the crossbedding is accentuated by rust colored and recess forming laminations.
- The Abrigo Shale is a mostly greenish brown, brown and black variably argillaceous metasiltstone and a very fine grained to fine grained thinly bedded to laminated metasandstone which can include calcareous metasiltstone. In some locations an argillite is present at the base.

Late Cretaceous and Early Tertiary Rocks

- The Rice Peak Porphyry (map unit Tkg) is a medium gray to greenish gray, low resistance intrusion with up to 30% sparse, chalky, white, relict plagioclase 2-3 mm and 1-3 mm biotite, both in a microcrystalline groundmass. Can contain up to 4% of K-feldspar phenocrysts up to 2 cm long and quartz-phyric phases. Can display strong foliation including stretched, brittle plagioclase phenocrysts and weak slatey cleavage development. Typically expresses as sills and dikes intruded into the Apache Group.

  - The Tkgm unit is described by Richard et al. (2000) as a light colored puraluminous muscovite granite that can contain garnet that also forms sills and dykes and is associated with the Rice Peak porphyry (Tkg)

- The Catalina Granite (map unit Tg) is a Tertiary porphyritic biotite and hornblende granite with pink orthoclase phenocrysts up to 4 cm long. The texture is hypidiomorphic granular. The plagioclase composition is anorthite, 26-32%. Xenoliths can be present.
- The unnamed Tertiary conglomerate (map unit Tsy) is a massive to crudely stratified, cobble to boulder conglomerate with clasts generally from 2 -30 cm in diameter but which can reach 2 m. Smaller clasts tend to be sun-angular and larger clasts sun-rounded. Clast composition includes Sierra Ancha diabase, Mescal limestone, Dripping springs Quartzite, Rice Peak porphyry, black siliceous hornefels and a fine grain equigranular leucogranite. Pinal schist and Oracle Granite are absent from the conglomerate.

Quaternary Sediments (Qtc)

- The Cordones Fanglomerate is a combination of Pliocene - Pleistocene alluvial fan consisting of poorly sorted sediments with 3-30 cm clasts of Pinal Schist, Apache Group, Sierra Ancha Diabase, Rice Peak Porphyry and local granites.

Sample Collection and Initial Preparation

Samples were collected from a road cut exposing approximately 4 meters of sediment. Sediment was removed by trowel and placed into gallon ziplock bags. The samples were transported back to the laboratory and left open to dry for approximately 5 days. After air drying, a portion of each sample was sieved through a 2 mm mesh to separate out the finer fraction for chemical analysis. Smaller portions of the < 2 mm fraction were oven dried at 105 ^{o}C prior to any analytic procedures.

ATR-FTIR Analysis.

A Fourier Transform infra-red (FTIR) spectrometer with an Attenuated Total Reflectance (ATR) attachment can be utilized to ascertain the amount of $CaCO_3$ in a soil sample. Loste et al. (2003) utilized ATR-FTIR to confirm $CaCO_3$ in solution

using the 1395, 868 and 712 (cm $^{-1}$) IR regions. These IR regions agree with Weir and Lippincott (1961).

A Nicolet iS5 FTIR spectrometer with an iD7 ATR attachment was utilized to create a calibration curve from sediment samples with known concentrations of carbonate. A sample of sediment from the surface of a debris flow on Signal Peak near Casa Grande, AZ was collected into a quart sized zip lock bag. The sample was sieved to 2mm using a 2mm metal mesh. A ten gram sample of the sieved portion was then treated for 4 hours, in a 100 mL beaker with 4 M HCl, to remove any existing calcium carbonate. The 10 gram sample was strained with filter paper, rinsed with DI H_2O, strained again and allowed to air dry for 24 hours after which it was placed into a drying oven at 105° C for 24 hours to remove all water.

A seven gram portion was ground to the consistency of flour using an agate mortar and pestle. An agate mortar and pestle was used in order to avoid contamination possible from other grinding methods. This portion was used to make eight, 1 gram samples containing known amounts of laboratory grade calcium carbonate from which a standard curve was generated.

Smaller samples of approximately 0.05 grams were taken from the mixes and placed onto the ATR-FTIR crystal for analysis. Each mix was analyzed three times using 32 scans at a resolution of 4 with automatic atmosphere suppression enabled.

A diagnostic spike in the 871-873 IR regions (Vahur et al. 2016) was utilized to create a standard curve by plotting the intensity (percent reflectance) against the known percentage of $CaCO_3$ in the samples (fig. 10). The 870 IR region was utilized because the 1400 IR region is shared between $CaCO_3$ and $MgCO_3$ (fig. 20). Additionally, the 712 IR region displayed significant randomness within the spectra of the standard samples.

Samples for analysis were also ground to a flour consistency in an agate mortar and pestle. Approximately 0.05 grams of each sample was placed onto the objective. Each sample was analyzed three times and the reflectance intensity at the 870 IR region was recorded for each. An average was calculated from the results of the replicates. Percent $CaCO_3$ was calculated for each sample utilizing the standard curve (fig. 10).

XRF Analysis

Portable x-ray fluorescence analyzers (pXRF) have been used to obtain elemental concentrations in various materials, to include geologic materials. Specifically, titanium, zirconium and niobium were of interest here. Previous research has used pXRF analyzers to quantify these elements (Figueora-Cisterna et al. 2011; Goren et al. 2011)

Samples were sieved through a 2mm steel mesh. Six grams of each sieved portion were placed into drying tins and dried for 24 hours at 105°C. 5.5 grams from each dried sample were placed into a 20 ml plastic scintillation vial along with three tungsten bearings for ball milling. Each sample was milled for 5 minutes using a Model 2601, Cianflone Scientific Instruments Co. Ballmill grinder. Each sample was then transferred into a pXRF analysis cup using 4.0 µ gauge polypropylene film in each cup. The samples were analyzed using a Niton Xl3t Goldd+ pXRF analyzer. Calibration was conducted using a multi-element reference sample. The "Test All Geo" function was utilized and set to 30 seconds for the Main, Low, High and Light ranges. Samples were placed face down in a lead shield stand for analysis.

Coarse and bulk samples of level 2410 were prepared using the same method but were analyzed using an Innov-X systems DP-2000, Olympus Delta pXRF analyzer due to equipment availability. Elemental abundances in the bulk sample were within error range of the both pXRF analyzers.

Sodium Dithionite Iron Extraction Analysis

A solution of sodium dithionite and sodium citrate can be used to extract pedogenic iron from soils (Mehra and Jackson 1960 ; McKeague and Day 1966). To prepare iron standards,

sodium dithionite solutions were made by adding 25 g of sodium citrate and 2 g of sodium dithionite to a beaker. $V=m/\rho$ was used to determine the total volume of the solutes resulting in 15.55 mLs. The solids were dissolved in ultra-pure H_2O and aliquoted to 118.29 mLs, using a 1000 mg/L iron standard solution, and ultra-pure H_2O, to create 10, 20, 30, 40 and 50 mg/L standards in acid washed bottles. The solutions were placed in a shaker for 24 hours. After 24 hours the solutions were diluted with ultra-pure H_2O into acid washed vials to create 1, 2, 3, 4 and 5 mg/L standards for maximum resolution. One blank solution (sodium citrate - sodium dithionite) was created and diluted to 1:10.

Two grams of the fine fraction (< 2 mm) from each sample was measured into acid washed centrifuge jars along with a sodium citrate, sodium dithionite solution. The sodium citrate, sodium dithionite solutions was made by adding 25 g of sodium citrate and 2 g of sodium dithionite to a beaker. $V=m/\rho$ was used to determine the total solid volume of 15.55 mLs. 102.74 mLs of ultra-pure H_2O were added to bring the solutions to 118.29 mLs. The jars were placed on a shaker for 24 hours. After 24 hours the samples were centrifuged for 15 minutes at 3600 rpm. After centrifuging 10 mLs of the extraction solution from each sample was pipetted into acid washed vials.

Readings for the creation of a standard curve (fig. 7) and sample analysis were done utilizing a Perkins Elmer 3100 Atomic Absorbance Spectrometer. Fuel utilized was an acetylene-air mixture of 1 unit of acetylene and 3 units of air. Operating conditions were: wavelength was set to 248.3 nm; slit was set to high and 0.2 units; operating current was 24 mA; mode was absorption; integration time was 0.3 seconds; replicates were set to 3. The bulb was adjusted until the gain stabilized at 140. The machine was zeroed utilizing the diluted blank solution. Each standard sample was read and the value recorded. 1 mL of each unknown sample was extracted into a beaker and diluted to 1:10 for initial atomic absorbance measurement. Sample 2400 resulted in an absorbance value that fell well above the limit of the curve. Trial dilutions were analyzed until the absorbance fell within the curve. The resulting dilution necessary for sample 2400 was 1:90.

Ammonium Oxalate Iron Extraction Analysis

An ammonium oxalate, oxalic acid solution can be used to extract non-crystalline, pedogenic iron from soils **(**McKeague and Day 1966). Standards were prepared by adding known amounts of 1mg/mL iron standard to four part ammonium oxalate (0.2 M) and three part oxalic acid (0.2 M) solutions (10mls) in opaque, acid washed vials. Standards were made to 1,2,3,4,5 mg/L

concentrations and placed into a shaker for 24 hours. Solutions were kept in the dark until analysis.

Samples were taken from the < 2 mm fraction previously sieved. 0.5 grams of each sample were added to 10 mLs of the ammonium oxalate, oxalic acid solution and placed on a shaker for 24 hours. After 24 hours samples were centrifuged at 3600 rpm for 15 minutes. Samples were kept in the dark until analysis.

Readings for the creation of a standard curve and sample analysis were done utilizing a Perkins Elmer 3100 Atomic Absorbance Spectrometer. Operating conditions were as noted above for the sodium dithionite extraction

Sample 2400 resulted in an absorbance value that fell well above the limit of the curve. Trial dilutions were analyzed until the absorbance fell within the curve. The resulting dilution necessary for sample 2400 was 1:50.

Empirical Dating

Dating of carbonates in the profile was done at the University of Texas El Paso using a Uranium-Thorium isochron approach (Ma et al. 2012). The age of the laminar cap (0.5 m depth) was determined to be ~ 121 ± 76 ka. The age of the lowest carbonate accumulation (3.5 m) was determined to be ~ 600 ± 3000

ka. However, the method used generally has an upper limit of approximately 400 ka years making the 600 ka age suspect, as suggested by the very large error (Dorale et al. 2004). Al^{26} (Jungers and Heimsath, 2018) were measured on samples of the basal gravel at the University of Arizona AMS lab. The results came back with no detectable Al^{26}. This result tentatively suggests a burial date for the basal gravel of approximately 3-5 ma given the amount of Be^{10} measured ($1x10^5$ atoms/g). However, this estimate is extremely uncertain due to the lack of a measurable exposure time for the basal gravel prior to deposition.

RESULTS AND DISCUSSION

Profile Description

The surface soil can be classified as a clayey-skeletal, mixed, superactive, thermic, shallow Ustalfic Petrocalcid (Soil Survey Staff, 2010). The colors were red, ranging from Munsell hues of 7.5 YR to 2.5 YR (Table 1). Soil texture ranges from a sandy clay loam at the surface to a clay at depth, with clay percentage ranging from 30 – 60% respectively. Rock fragments averaged around 45% (gravels and cobbles) throughout the upper 35 cm. There are significant clay films between 18-35 cm. A cemented laminar cap of about 2-5 cm thick underlies the

argillic horizon. Below this, the soil lightens dramatically due to higher accumulations of carbonate (15-25%). Below the cap is a lens of larger gravels and cobbles approximately 10-12 cm thick. The rock fragments then return to a character similar to the surface soil. At approximately 2.35 m of depth, there is a sandy, lens of redder material approximately 3 – 5 cm thick. Below this, the profile contains larger cobbles and is marked by to separate accumulations of carbonate. The upper (from about 2.5 to 3 meters) contains roughly 56% carbonate. From 3.5 to 4 meters, the profile contains roughly 44% carbonate. Below 4 meters is the basal gravel. Assuming a bulk density of 2.0, and using an average carbonate accumulation of 27.4%, an estimate of total carbonate accumulation in the profile comes out to be approximately 2192 kg/m^2 of carbonate given a meter square column that is 4 meters in depth. That translates to approximately 548 kg/m^2 of carbonate in a cubic meter of this sediment.

Carbonate Content

The two analytical methods of quantifying carbonate content gave noticeably different results. Sample 2401, the petrocalcic laminar cap, resulted in a $CaCO_3$ percentage of about 91 using the digestion method but only 72 using the ATR-FTIR method (figs. 11,12). The likely reason for this is that the HCl used in the gas method would also dissolve other carbonates, such as

magnesium carbonate, thus producing more gas pressure. Both $CaCO_3$ and $MgCO_3$ spike in the 1400 IR region in the ATR spectra (fig. 20). A standard curve built from intensity in the 1400 IR region resulted in a value of approximately 85% for the laminar cap suggesting that the presence of other carbonates does account for the difference between the FTIR and digestion method results.

Carbonate Distribution and Accumulation Rate

The Saddlebrooke profile may have up to two bimodal distributions of carbonate which would be in line with the McFadden and Tinsley (1985) model. In the FTIR data (fig. 11), there is an increase in $CaCO_3$ accumulation under the laminar cap that is preceded by a zone of lesser $CaCO_3$ accumulation. However, the depths in the Saddlebrooke profile are greater than the McFadden model projects. The laminar cap sits at 0.5 meters depth while the subsequent accumulation is 1.5 meters deep. Given the fact that the alluvial fan is a remnant fan, it may be hard to explain the depth to carbonate at Saddlebrooke via continued deposition, post accumulation. More likely it is simply the difference in time. The McFadden model was based on a Quaternary deposit that was 30 ka. The Saddlebrooke laminar cap dates to 121 ka such that is was exposed to much wetter conditions over the last glacial maximum (LGM), that may account

for deeper carbonate accumulation. It is also possible that much of the original soil surface has been eroded since the emplacement of the laminar cap such that the depth of the cap is reported shallower that when originally deposited.

An estimate for carbonate accumulation can be made. Assuming the 600 ka date for the deepest carbonate accumulation is correct, a very rough estimate of approximately 3.5 kg of carbonate per 1000 years can be made. Because approximately 12% of the mass of $CaCO_3$ is carbon, approximately 0.42 kg of carbon would be sequestered every 1000 years in a meter square column. Of course the reality of this sequestration would not be so linear but would have a more punctuated nature over the 600,000 year span of time. However, given the Al^{26} result, this estimate may be quite far off. If the Al^{26} does indicate a burial date of $\sim \geq 4$ ma, then the lower portions of the profile may be much older. For example, it becomes possible that only the material above the red band is Pleistocene in age and the material below the red band may be Tertiary basin fill. This older date would reduce the overall accumulation rate significantly.

Iron Data

At 0.2 m the amount of pedogenic, crystalline iron is very high relative to the rest of the sequence with up to 21.9% extractable Fe (fig. 8) indicating a significant degree of

chemical weathering. The laminar cap underlying the argillic horizon dates to 121 ka. Because petrocalcic horizons are developed via leaching, it is reasonable to suspect that the Ustalfic Petrocalcid is approximately also 121 ka and likely significantly older given its correlation with the 1.8 – 2.0 ma high stand surfaces in other basins in the region (Jungers and Heimsath, 2015; 2018). This indicates that the uppermost soil was developing during the period that contains the LGM, and was subject to much wetter conditions (Ibarra et al. 2014). Evidence from studies of Pleistocene pluvial lakes suggest that much wetter conditions existed in this area during the LGM that were associated with a southward shift of storm tracks, due to the presence of ice sheets in the north (Enzel et al. 2003 ; Ibarra et al. 2014). While the data from the lake studies is much younger than the bulk of the chronosequence, they still speak to the effects of the ice sheets on atmospheric circulation. In these studies wetter conditions include an approximate 50% reduction in evaporation (Enzel et al. 2003) as well as an approximate 50%- 75% increase in precipitation (Ibarra et al. 2014).

At 2.35 m there is a notable spike in extractable iron up to 0.24% suggesting increased weathering and a period of stability with that surface in place for long enough for reddening to occur. Below the red band, iron content is

generally lower. Because the low iron percentage could be due to the accumulation of carbonates, $CaCO_3$ was mathematically removed assuming a 100 g sample and using the following equation:

$$(M_{Fe} \div (\frac{M_S - M_C}{100})) \times 10000 \quad \{Eq.\ 7\}$$

Here M_{FE} is the mass of extractable iron, M_S is the sediment mass and M_C is the carbonate mass. The results were plotted next to the iron values that still contain $CaCO_3$ in the soil (fig. 9) This revealed slight increases in crystalline iron up to 0.28% at 2.5 m and up to 0.34% 3.5 m. These increases in crystalline iron suggest that the material underwent greater weathering and may represent periods of past surface stability.

Eolian Proxies

The ratio of titanium to zirconium (Ti:Zr), and the ratio of zirconium to niobium (Zr:Nb), are useful proxies in determining the amount of eolian material in a soil or sediment package (Pelletier et al. 2011), as long as the geochemical signatures of the sediment and dust are distinct from one another. These elements are generally immobile in typical weathering conditions (Reheis et al. 2009), meaning that as other elements are leached away, these elements will concentrate. When numerous surfaces are subject to eolian

erosion, the resulting dust can take on a unique isotopic signature of immobile elements. Subsequently, when deposition of this eolian material occurs, the elemental signature of the dust can imprint on the local sediments. Data from the XRF analysis was used to compare deviations from a dust line and a parent material line throughout the profile (figs. 13-16). This was done using Ti:Zr and Zr:Nb. The Ti:Zr ratio of the dust (Ti:Zr ~ 32.5) was taken from Fischer et al. (2017), while the Zr:Nb dust ratio (Zr:Nb ~ 23) was taken from Pelletier et al. (2011). The parent material ratio used in both was taken from the basal gravel (sample 2410) located at the Saddlebrooke site.

The Ti:Zr method resulted in only two depths at which measured increase in $CaCO_3$ tracks with Ti:Zr movement towards the dust line (figs. 13,15). Those depths are 1.2 m and 2.2 m. At every other depth, the trends are opposite, $CaCO_3$ increases but Ti:Zr moves away from the dust line. The Zr:Nb method resulted in more depths with a positive correlation between $CaCO_3$ accumulation and movement of the elemental ratio towards the dust line (figs. 14,16). These depths are 1.2 m, 1.8 m, 2.5 m and 3 m. Additionally, there is a correlative trend between depths 1.2 m and 2.2 m where carbonate accumulation tracks with the proxy ratio. The rest of the depths again show opposing trends. Furthermore, at depths below 2.35 m there are two large spikes in carbonate that have no correspondence with the dust

proxies. At first glance this seems to suggest no correlation between the eolian deposition and the carbonate accumulation, however several factors make drawing a conclusion difficult.

A lag effect may account for the disparity between the eolian proxies and carbonate accumulations. If dust carried carbonates as well as immobile elements it stands to reason that over time the dust accumulation would be leached of soluble material and become enriched in immobile elements. This should result in zones enriched in immobile elements overlying zones of carbonate accumulation. Some portions of the Ti:Zr data might suggest such a scenario (figs. 13,15) in the upper half of the profile, there is a steady increase in Ti:Zr between the depths of 0.8 and 2.35 m. This steady increase is followed by a spike in $CaCO_3$ at 2.5 m. The possibility is that enough eolian carbonate could have been brought in to be leached downward and produce the spike seen at 2.5 m. This scenario is undermined by two observations. First, the opposite trend is visible in the Zr:Nb proxy. Zr:Nb decreases to its lowest point (aside from the petrocalcic horizon) prior to the large spike in $CaCO_3$ at 2.5 m depth. Secondly the spike in $CaCO_3$ lies beneath the "red band." The presence of the red band suggests a buried horizon. The thinness of the band could also suggest that it may have undergone erosion prior to its subsequent burial. If this is the case, then the sediments from which the underlying calcic

horizon was derived may have eroded away, and the current concentrations of eolian proxies have nothing to do with what lies beneath them.

In an attempt to understand why the trends in the two sets of proxies are so different, the concentration for each of the 3 elements were plotted along with the parent material concentration for each (fig. 19). What is notable is that the general shape of the Zr:Nb graph (fig. 18) does not resemble either zirconium or niobium alone. However, the general shape of the Ti:Zr graph (fig. 17) does strongly resemble the shape of the titanium graph. This indicates that changes in titanium concentration are the primary driver of changes in the ratio. Also, the concentration of titanium throughout out the profile falls below the concentration of the parent material at all levels except two, 0.2 m and 2.2 m, whereas the concentration of zirconium remains above or at the concentration of the parent material (except in the laminar cap). There are a few possible explanations.

One possible explanation is preferential erosion of the parent materials feeding the alluvial fan. Changes in the sediment sources delivered to the Cordones surface could affect the data in three ways. It is possible that conditions in the Catalinas could have resulted in the weathering and erosion of rocks higher in titanium which ended up deposited as the basal

gravel. Secondly, preferential erosion could explain the spikes in calcium carbonate. In general, sedimentary rocks weather much more readily than igneous rocks, and the Mescal Limestone is present in the watershed feeding the alluvial fan. Packing the sediment with material low in titanium, relative to the basal gravel, would explain why the titanium concentrations fall below the parent material line. Additionally, this could explain shifts in titanium in the upper portion of the profile. If the stream was gradually shifting in the mountain watershed and eroding different rocks, this could potentially lead to shifts in titanium concentration in sediments deposited downstream. Preferential erosion could also explain the higher zirconium concentrations, if rocks high in zirconium were being preferentially eroded at the right time. However, since the zirconium remains steady, this again requires an unlikely erosional shift from one rock source to another which are equal in zirconium levels.

A second option is an eolian source which is low enough in titanium to drive the titanium concentrations down, but high enough in zirconium to keep the concentrations above the parent material line. However, this is hard to reconcile with the Ti:Zr throughout the profile. If the dust source is low in titanium, then the steady increase in the ratio between 0.8 m and 2.2 m (fig. 17) would have to be explained by a significant reduction

in zirconium. That is not what is observed. Instead, zirconium remains fairly steady, and increases at 2.2 m. Another eolian possibility is a shift from one dust source to another that differed enough in titanium concentration to drive the observed change in the ratio. Given that the basis for using titanium and zirconium as eolian proxies relies on their immobility leading to their concentration in surficial sediments (which can be picked up by the wind) it seems unlikely that eolian material with such a specific low titanium concentration would be the cause. Additionally, zirconium levels change very little in the upper half of the profile. This would require a change to a new dust source that differs in titanium content, but remains the same as the last in zirconium content.

A third option is that titanium in this system is more mobile than in others. A potential mechanism could be uptake by plants, especially given climates where wetter conditions allow for greater plant growth. However, the data may not fit this scenario. Moving up profile from depth 2.2 m to depth 0.8 m is moving forward in time towards the age of the laminar cap age of 121 ka, which is an interglacial (fig. 22). As conditions got warmer and more arid, plant life likely waned and thus any titanium uptake should hypothetically wane. Instead, the opposite trend appears. Moving closer to that 121 ka cap from depth, titanium reduces in concentration. The possibility of

titanium being preferentially removed in the lower half of the profile, where low concentrations of titanium correlate to spikes in carbonate, is also unlikely. Zirconium concentration also reduces in the lower half of the profile. Both titanium and zirconium show a significant decrease from 2.2 to 2.5 meters. Below the red band, where carbonate is high these elements are lower and where carbonate is low, these elements are higher. Ti:Zr follows the same trend. The observation that both elements follow this trend suggests that the addition of carbonate taking up space in the profile is what is causing both elemental concentrations to reduce. However, given that carbonate concentration recorded in the deeper spikes takes up only approximately half of the volume of material, the ratio of the elements remains intact. In effect, there is enough volume left to obtain a useable ratio of titanium to zirconium.

A fourth consideration is a low zirconium dust source. Zircon crystals are dense and this might cause them to winnow out of an air columns as it transports a load of dust. In this scenario, the high concentration of zirconium in the upper half of the profile could be explained as a lithological feature. That is, the lithological parent material being deposited in that portion of the profile may have been higher in zirconium, and that immobile element became enriched in situ. In this scenario, titanium becomes the dust signal and introduction of

eolian titanium to the system drives the change in the elemental ratio.

Given these uncertainties with titanium, the Zr:Nb proxy may be a better choice for determining eolian input. Niobium is a very rare element with an average abundance in the earth's crust of about 8 ppm (Schulz et al. 2017). Fluctuations in the weathering of different rocks in the Catalinas would be unlikely to result in concentrations of niobium on the orders of approximately 25 ppm and 35 ppm that are observed in the data, however preferential erosion is still a possibility that could affect zirconium concentrations. Between 1.8 and 2.2 meters, zirconium concentration only rises about 7 ppm whereas niobium concentrations jump about 17 ppm (fig. 19). This spike in niobium drives the Zr:Nb away from the dust line. At 2.5 meters, the Zr:Nb increases and that increase correlates to the carbonate spike at the same depth, however, zirconium sits barely 2 – 4 ppm over the parent material line at that depth whereas niobium falls below the parent material line at that depth.

To better understand the effect of carbonate accumulation on immobile element concentrations, the immobile element portions were recalculated after mathematically subtracting the mass of carbonate. Using a hypothetical 100 gram sample at each depth, the following equation was utilized:

$$(M_{IE} \div (\frac{M_S - M_C}{100})) \times 10000 \quad \{Eq.\ 8\}$$

Here M_{IE} is the mass of the immobile element, M_S is the mass of the soil sample and M_C is the mass of carbonate. The results produced plots of immobile element concentrations that were markedly different from the concentration plots that include the carbonate fraction (fig. 21). Above the red band, titanium retains its increase in concentration with an increase in depth but now shows greater increase beyond the parent material concentration. Zirconium concentration remains greater than the parent material concentration, and now shows a trend of decreasing with depth. Zirconium also shows presence at the depth of the laminar cap. Niobium concentrations now fall at or significantly above the parent material concentration through the whole profile and maintains its anomalous spike at 2.2 meters depth. Niobium also remains significantly higher than the regional dust concentration of 10 ppm reported by Pelletier et al. (2011). Lastly, niobium has a significant concentration at the depth of the laminar cap. All three immobile element concentrations show a decrease from 2.2 meters to 2.35 meters.

The very high concentrations of niobium, relative to dust and crustal estimates, require the assumption of a dust source concentrated very heavily in niobium if it is to be used as an

eolian proxy. This possibility is not without some support. Dunbar and Hervig (1992) report niobium concentration values that commonly exceed 20 ppm, with some measurements exceeding 50 ppm, for the Bishop Tuff in California. Izett et al. (1988) report that the largest eruption of the Bishop tuff occurred ~ 0.74 ma and left traces as far as Nebraska. Due to the high niobium concentrations of this volcanic deposit, and its potential reach, both the anomalous niobium spike and generally higher concentrations can be explained. The general high concentrations can be explained by dust enriched in niobium being produced from surface sediments effected by the Bishop Tuff. Though correlation to the Bishop Tuff would have to be proven with other evidence, the fact that the concentrations of Ti and Zr also exceed the parent material concentrations create a fairly clear eolian influence on the accumulation of the laminar cap.

Below the laminar cap, niobium and zirconium both decrease while titanium increases. Given the high concentrations of zirconium and niobium, and given that the Zr:Nb proxy does track with carbonate concentration, the Zr:Nb can be taken as a good indicator of eolian input below the laminar cap. The increase in titanium can still be explained by an erosional shift in the catchment. Just above the red band, at 2.2 meters, all three elements increase. Niobium increases drastically to over 40 ppm.

This may indicate a unique depositional event, such as Bishop Tuff eruption, or a period of more intense eolian deposition.

Below the red band, titanium remains below the concentration of the parent material but displays an increasing trend between 3 and 4 meters depth. Zirconium shows a significant spike at 2.5 meters depth and has a trend of increase between 3 and 4 meters. Niobium shows small increases at 2.5 and 3.5 meters. All three immobile elements show an increase at 2.5 meters that corresponds with the largest accumulation of carbonate below the red band.

At 2.5 meters the immobile element concentrations and carbonate concentration increases. At 3 meters depth, both decrease, only to increase again at 3.5 meters. This tracking between the carbonates and the immobile element concentrations may indicate some eolian influence below the red band as well. Both the negative correlation displayed by Ti:Zr, and the positive correlation displayed by Zr:Nb at 2.5 meters is driven by the significant increase in zirconium. Because this increase exceeds regional dust values, it may indicate the influence of another source of zirconium. At 3.5 meters, both immobile element ratios decrease while carbonates increase which suggests a lack of eolian influence on the carbonate accumulation at this depth. Niobium and zirconium both remain higher than the parent material concentration, however. Given that titanium

concentrations may be primarily driven by erosion in the catchment, the possibility of some eolian influence on the lowest carbonate accumulation cannot be ruled out.

Groundwater and Calcium Bearing Rain

The profile analyzed is in the top 4 meters of the Cordones Fanglomerate. The channel adjacent drops approximately 33 meters in elevation relative to the surface of the profile. Given the poorly sorted sediments of the alluvial fan, it is not likely that precipitation of carbonates dissolved in ground water can account for the accumulations observed.

McFadden and Tinsley (1985) provide rainwater Ca^{2+} estimates of 0.5 to 2 ppm for the Mojave Desert. Assuming that Pleistocene increases in rainfall, and Ca^{2+} concentrations, estimated for the Mojave apply to southern Arizona, an estimation of calcium contributed by rainfall can be made. Current precipitation for Tucson Arizona is approximately 30.3 cm of rain annually (US Climate Data, 2019). Ibarra et al. (2014) suggest increases of 50-70% of annual precipitation during the LGM. Assuming the low end of 50% more rain would yield approximately 45.5 cm of annual rainfall in this area. This would equate to approximately 455,000 cm^3 of water per meter or 455,000mLs or water per square meter. If 0.5 ppm of that was calcium, then given approximately

22.75 mLs of Ca^{2+} would be left by rainfall annually. At a density of 1.55 g/cm^3 that is approximately 14.7 g of calcium annually in a meter square area. Assuming continuous high rainfall between the LGM and the beginning of the Holocene (approximately 16K years); at a soil bulk density of 1.8 approximately 13% of the mass would be calcium delivered by rainfall in a soil comprised of approximately 50% carbonate. At a higher bulk density of 2.5, approximately 10% of the mass would be calcium brought in by rainfall. These values are similar to estimates made by McFadden and Tinsley (1985) in which approximately 15% of the carbonates in the Mojave soils might be derived from rain deposited calcium. Depending on the Ca^{2+} concentrations and actual increases in rainfall during the LGM, rain delivered calcium could account for a significant portion of the carbonate accumulation.

CONCLUSIONS

To draw conclusions concerning the primary source of carbonate accumulation (eolian vs parent material) consideration is given to potential climate regimes recorded in ice records (fig. 22). At ~121 ka, there was an interglacial at which time conditions would have been warmer with less precipitation. Given that both Ti:Zr and Zr:Nb, in the Ustalfic Petrocalcid, have values significantly higher than the parent material the source

of carbonates that formed the laminar cap are concluded to be eolian.

The disparity between the two proxies in the upper portion of the profile, below the laminar cap is likely due to titanium concentration being driven by differential erosion in the catchment. The very high levels of zirconium and niobium, and positive correlation between carbonates and Zr:Nb, indicate strong eolian influence on the carbonate accumulations between 0.5 and 2.35 meters.

Below the red band, both immobile element ratios show negative correlation with the carbonate accumulations. At 2.5 meters, this drop in the Zr:Nb is driven by an anomalous spike in zirconium that exceeds the dust estimates given in literature. This high concentration of zirconium may indicate a zirconium source other than dust which makes the influence of eolian material uncertain.

In summary, three depositional events are concluded to be present in the Saddlebrooke profile. The upper half of the profile (above the red band) is material that forms one depositional package. This material bears a signature of changing amounts of eolian deposition which resulted in the formation of the petrocalcic cap and heavily influenced the carbonate content below it.

Below the red band, accumulations of carbonate do not track

with increases in the eolian proxies Ti:Zr and Zr:Nb, though there remains a potential for eolian contribution in the high niobium and zirconium concentrations. Additionally, the increases in carbonate do track with increases in weathering indicated by pedogenic iron. These results indicate that carbonate accumulation at 2.5 meters is likely due to a combination of eolian input and weathering of calcareous rocks in the catchment. The carbonate accumulation at 3.5 meters is likely due primarily to the weathering of calcareous rocks.

FIGURES AND TABLES

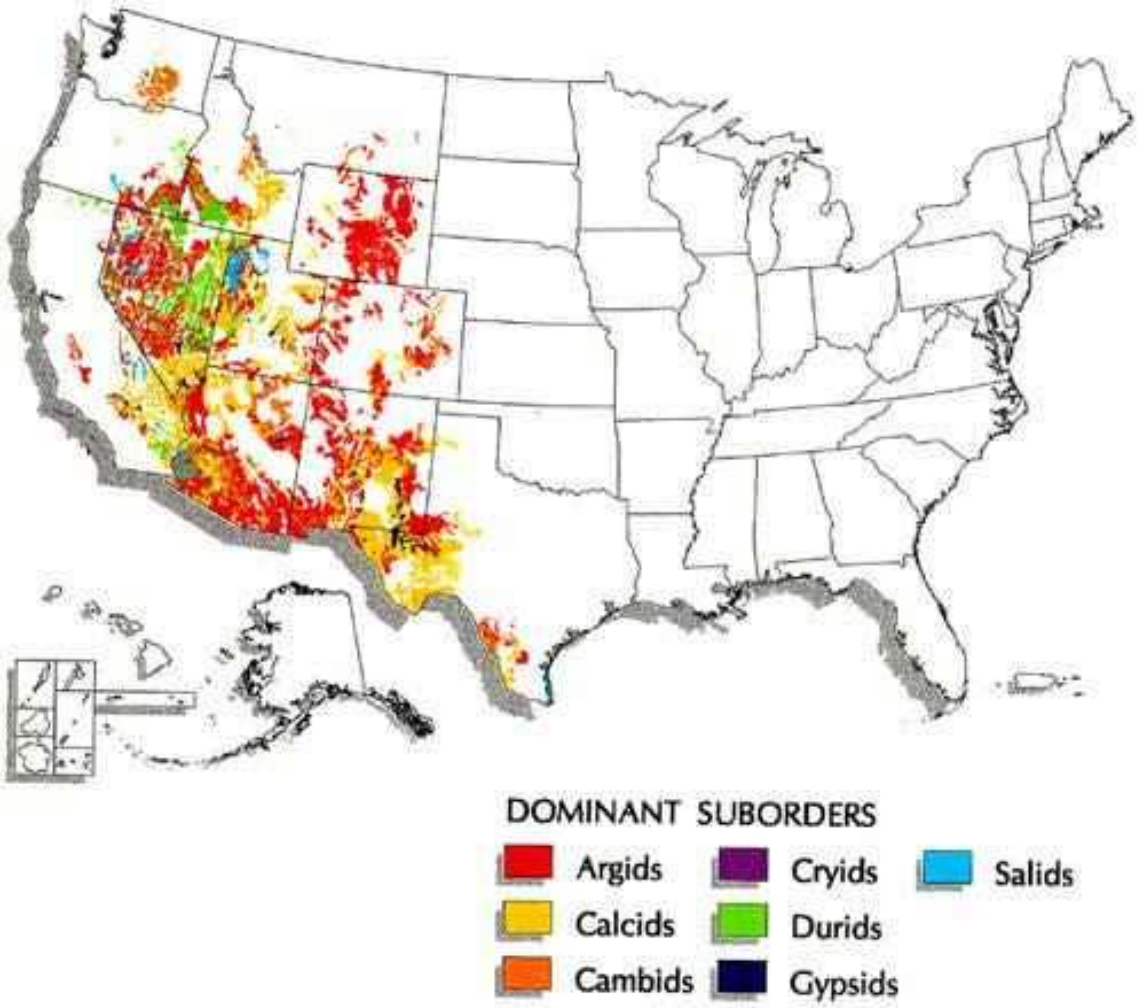

Figure 1: Dominant soil suborders focused on the southwest U.S. (NRCS 2019).

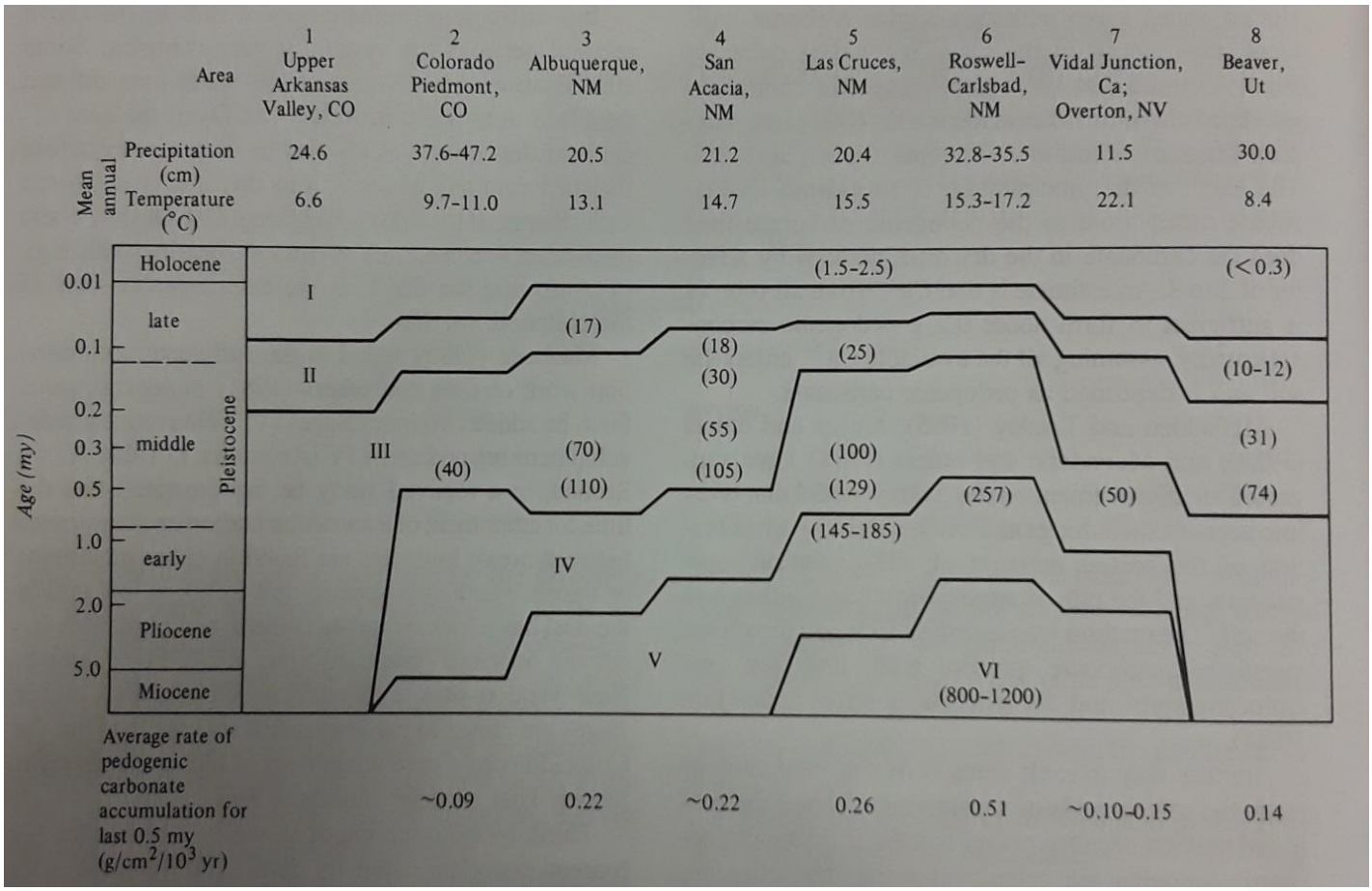

Figure 2: Carbonate stages in relation to age and climate. Taken from Birkeland (1999).

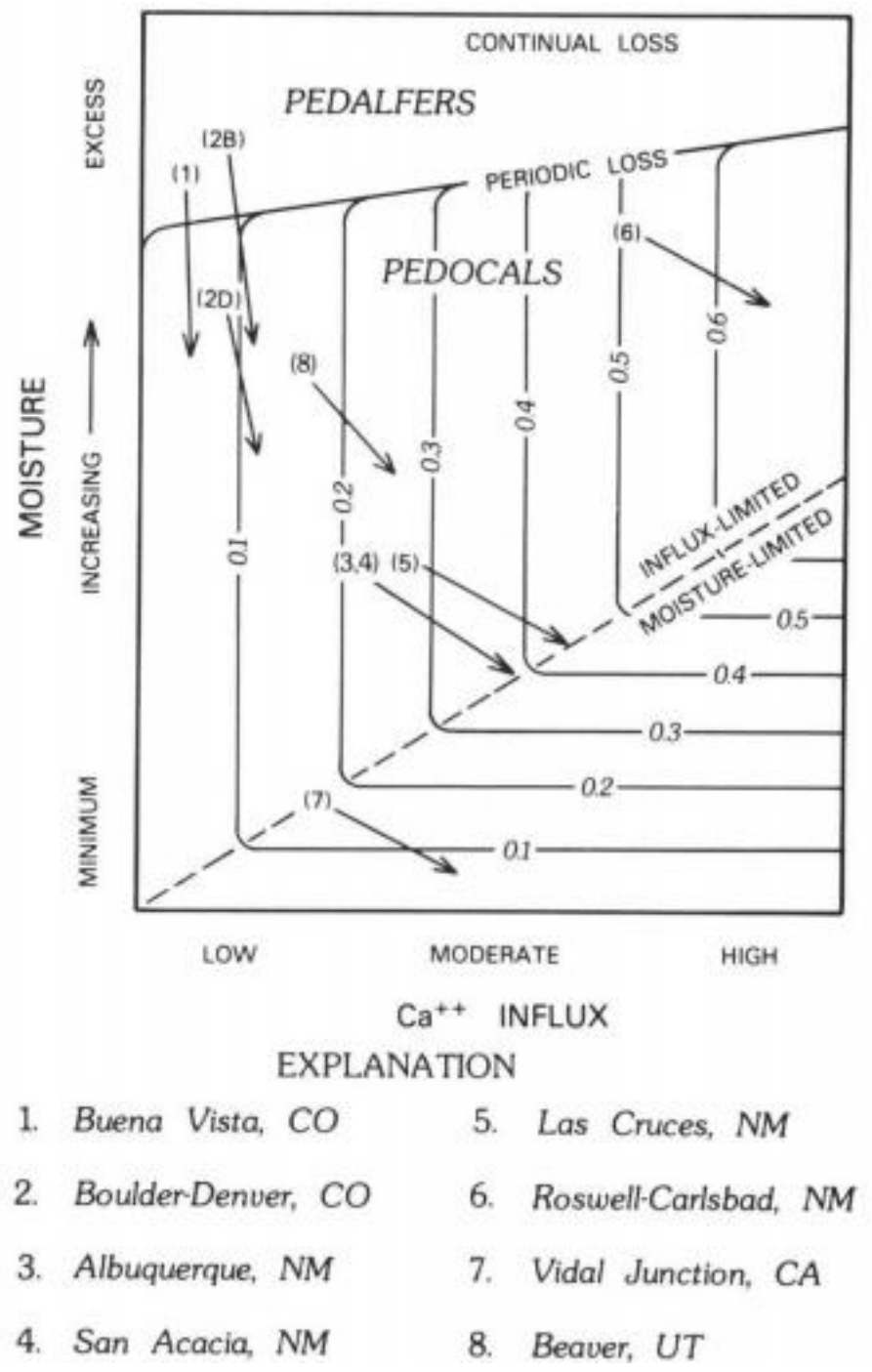

Figure 2: Relationship of influx of free calcium to precipitation. Taken from Machette (1985).

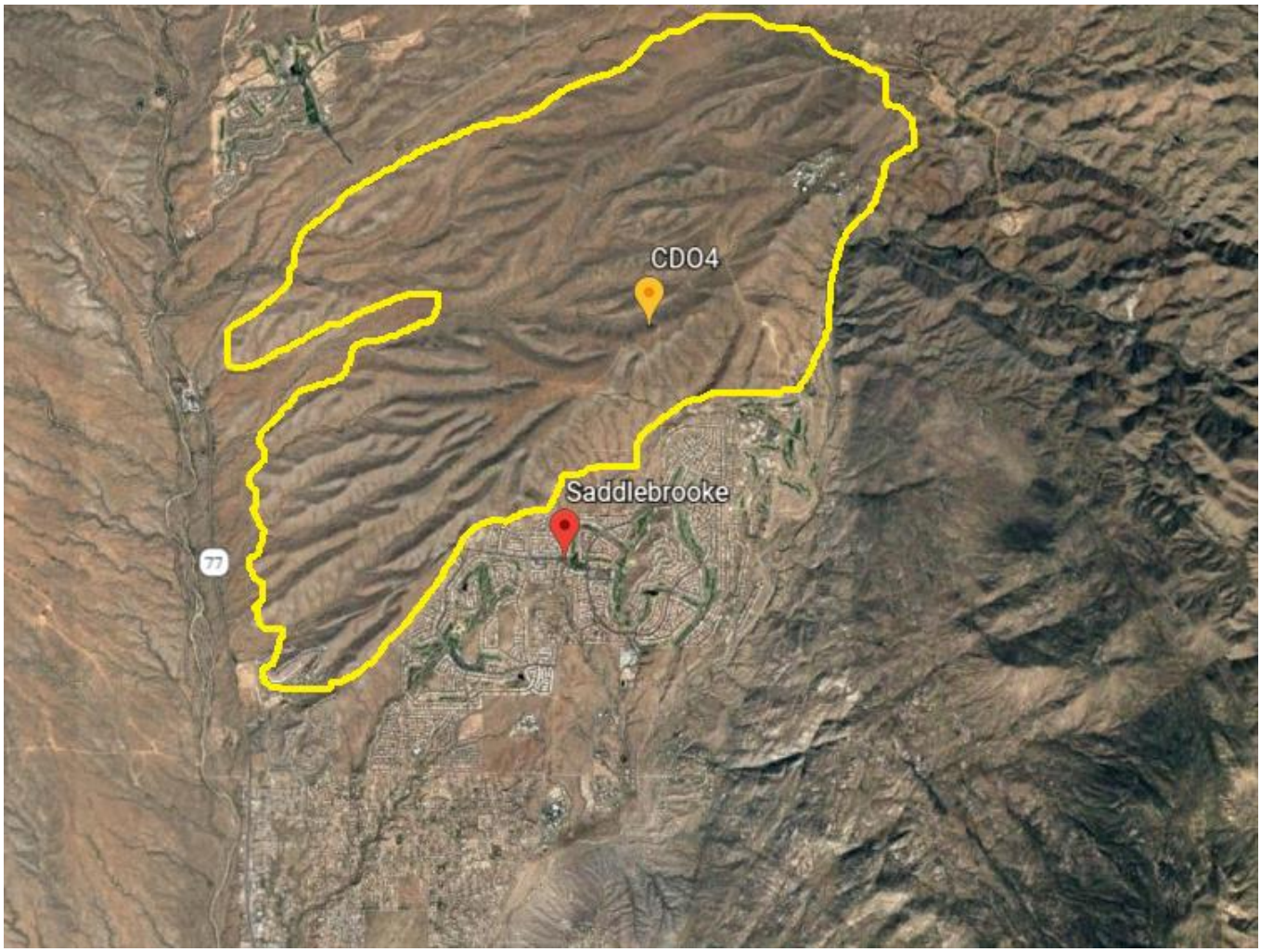

Figure 4: Location of the soil profile within the upper sediments of the Cordones Fanglomerate near Saddlebrooke, AZ.

Figure 5: Photograph of the profile exposed by the road cutting through the top of the Cordones fanglomerate. The petrocalcic laminar cap sits just below the reddened soil at the top. The red band is visible approximately halfway down the profile. Two accumulations of carbonate, separated by a gravelly deposit, are visible in the lower half.

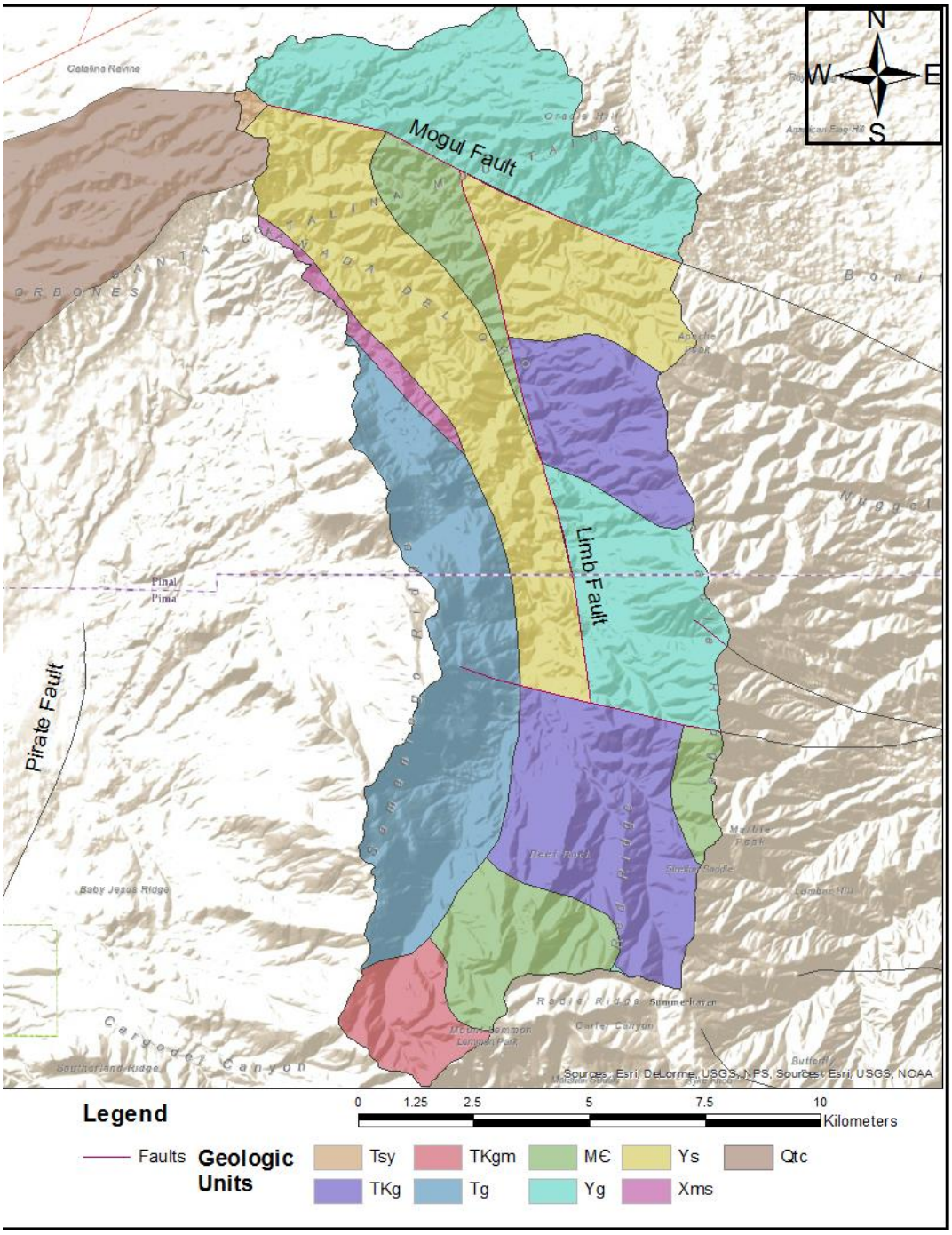

Figure 6: HUC 12 Canada Del Oro watershed. Map was generated using geospatial data from the Stroud research group (2018) and Arcmap Raster data.

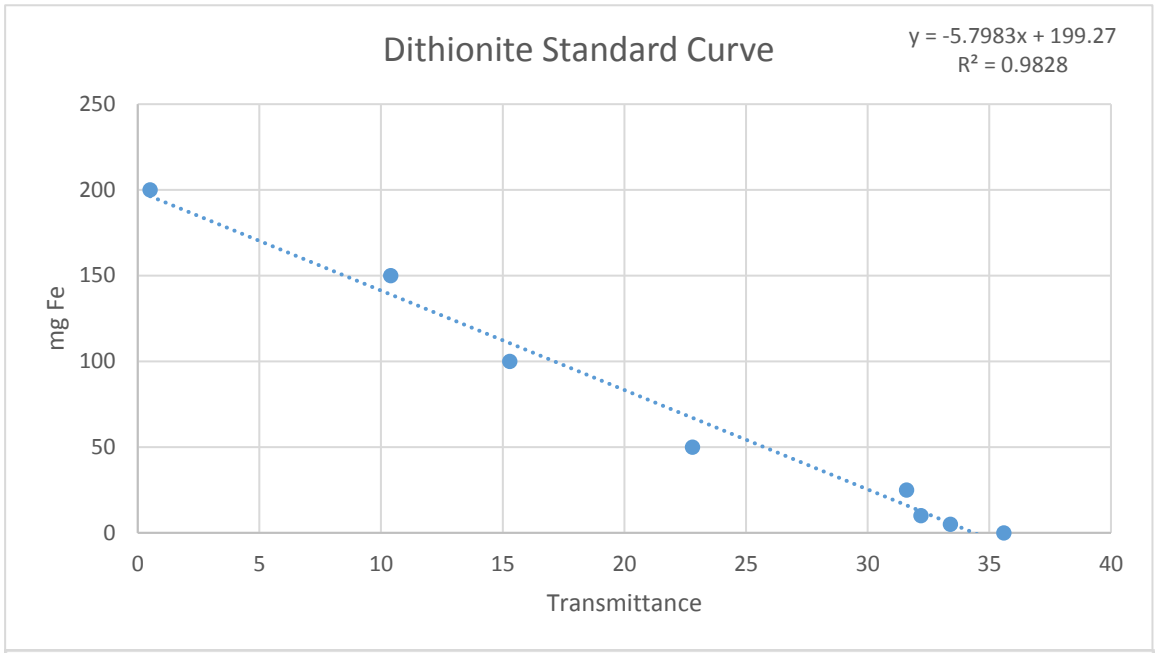

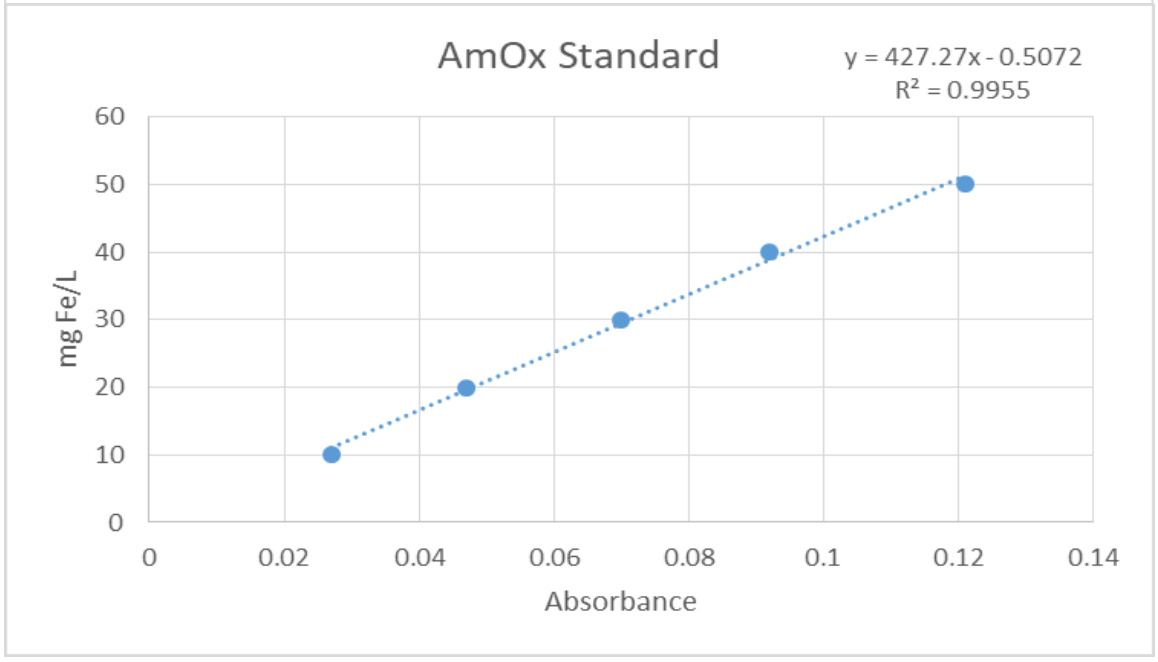

Figure 7: Standard curves used to calculate pedogenic iron concentrations for each sample.

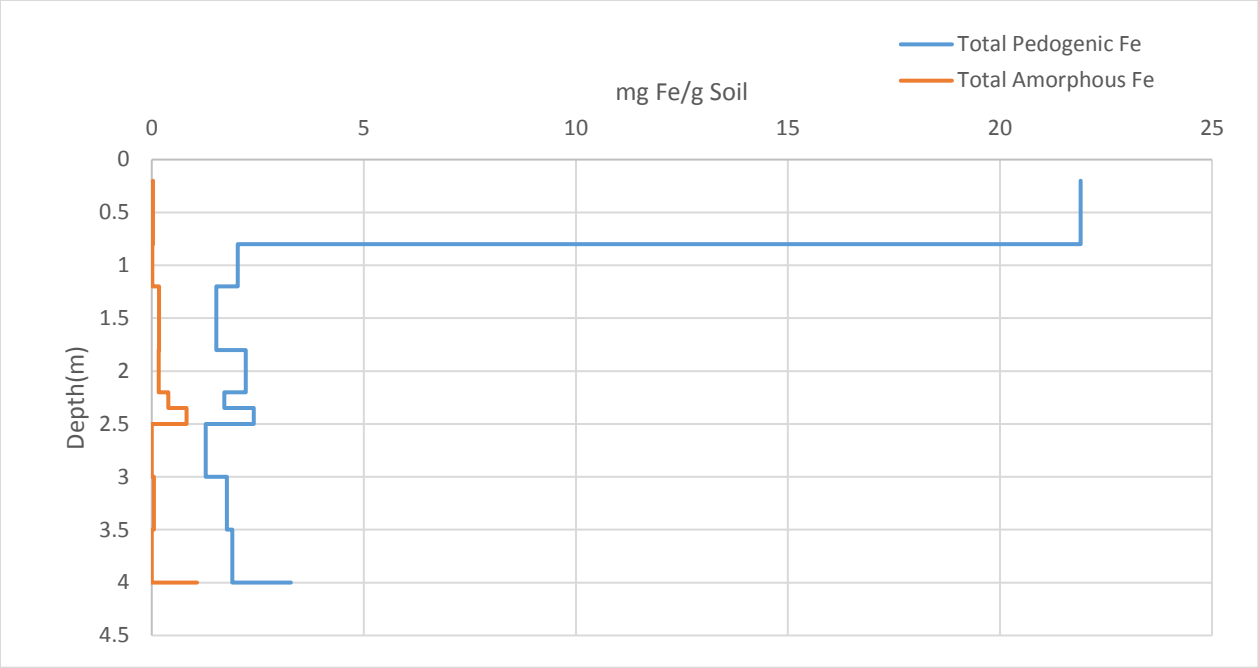

Figure 8: Comparison of iron obtained from the Sodium Citrate – Dithionite extraction and the Ammonium Oxalate – Oxalic acid extraction. Shows portions of iron that are pedogenic crystalline and amorphous.

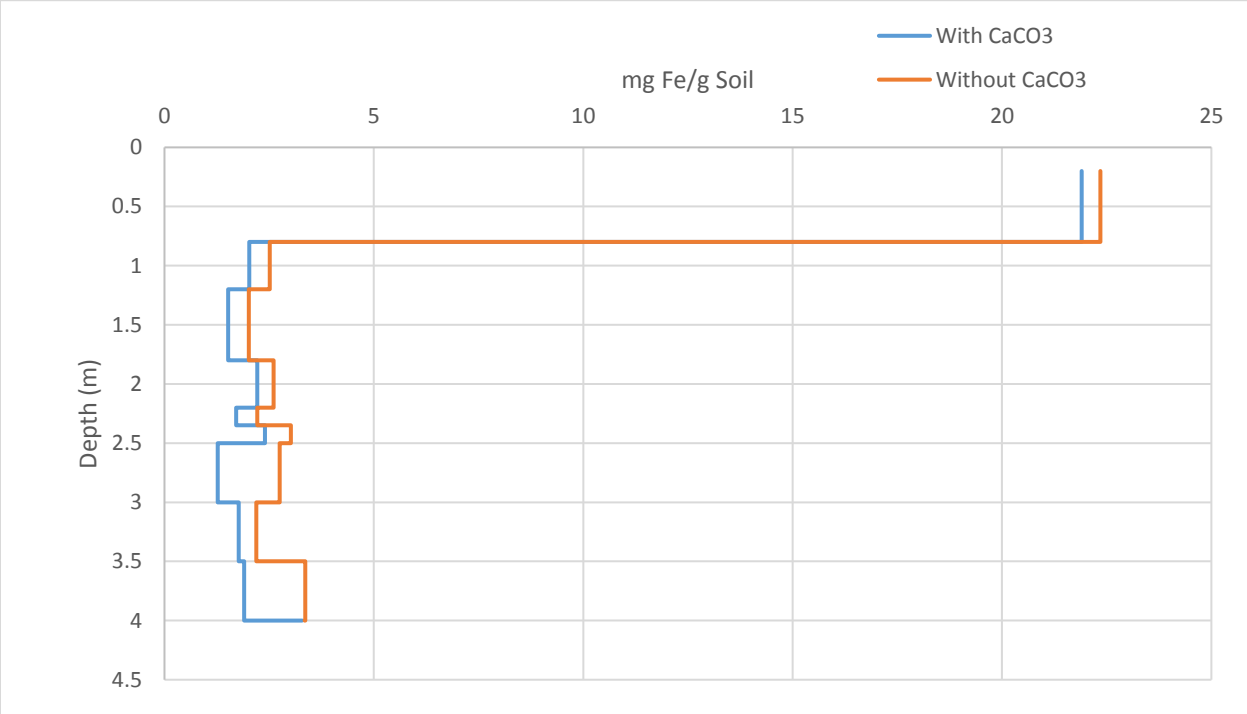

Figure 9: Values of total pedogenic iron compared to values with the mass of carbonate mathematically subtracted. Increases at depth are present but total pedogenic iron concentration remains small.

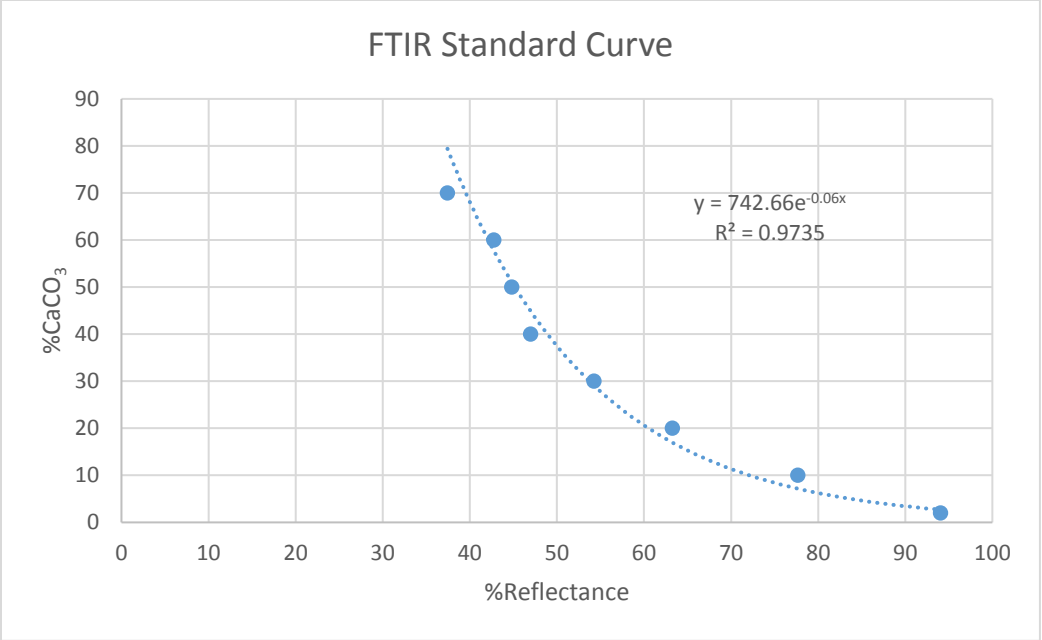

Figure 10: Curve used to calculate %CaCO3.

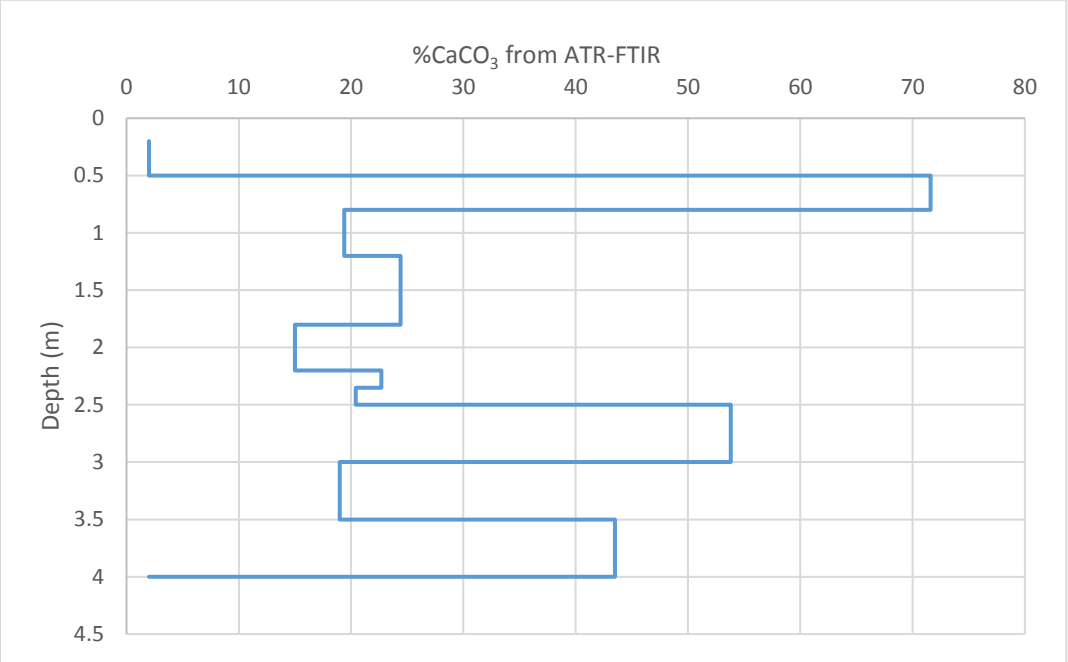

Figure 11: %CaCO3 derived from ATR-FTIR analysis.

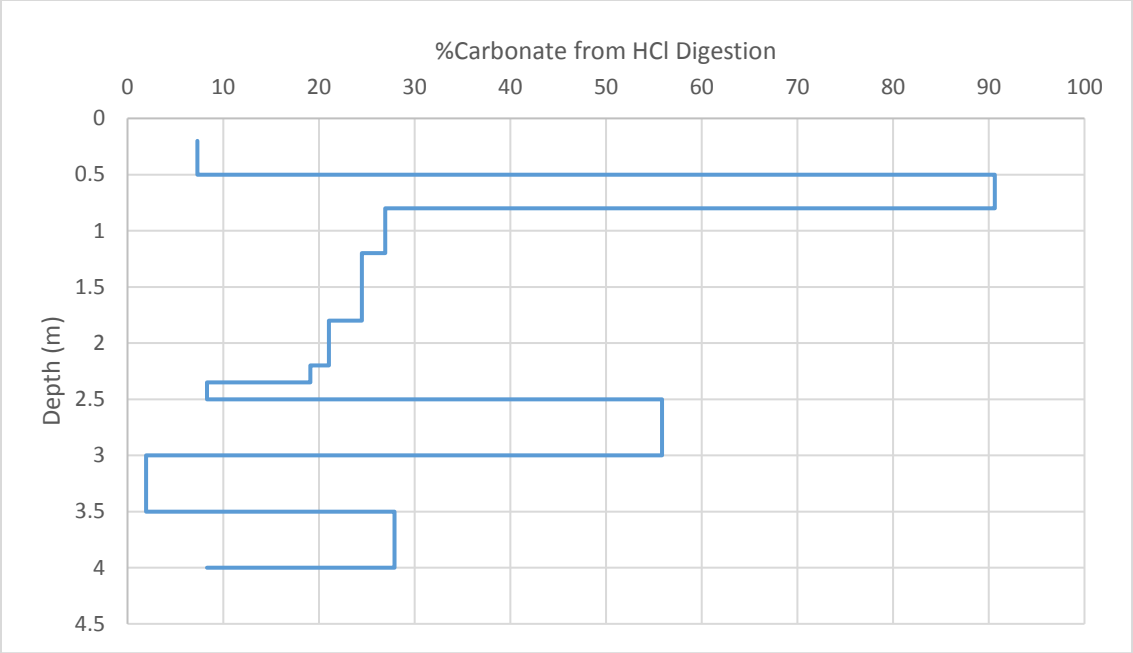

Figure 12: %Carbonate derived from the HCl digestion method.

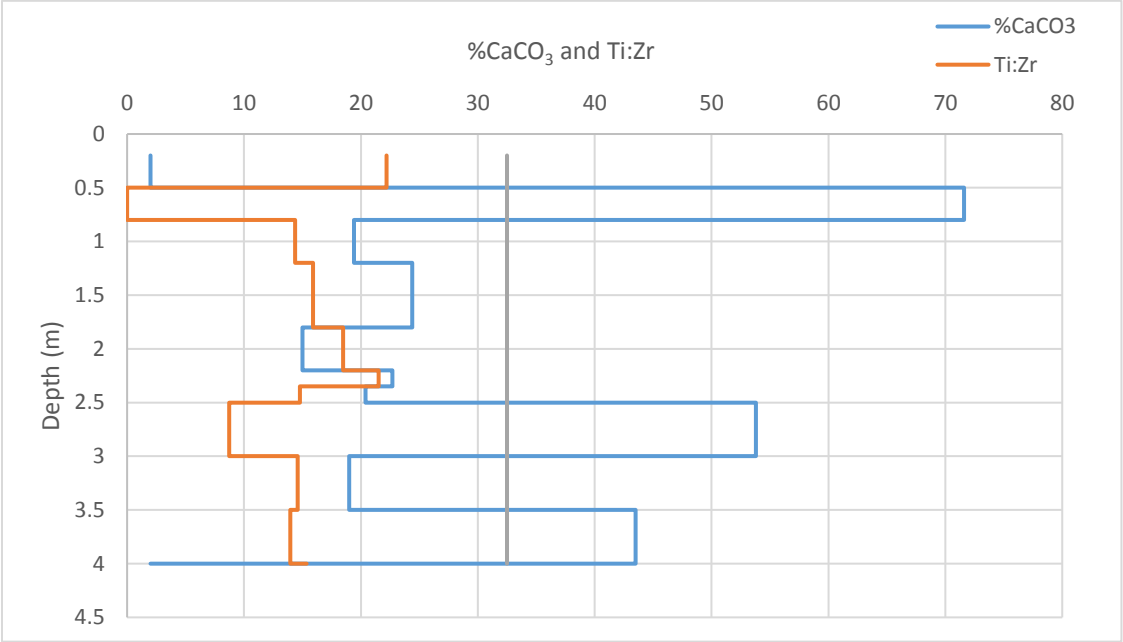

Figure 13: Ti:Zr plotted against %CaCO3 from FTIR and a Ti:Zr value for regional dust. Regional dust ration taken from (Pelletier et al. 2011). The petrocalcic, laminar cap is at 0.5 meters depth. The zero value for Ti:Zr is due to the cap being comprised primarily carbonate. Correlation between increases in the Ti:Zr (eolian proxy) and carbonate accumulation is weak. A potential lag between high Ti:Zr at depth 2.2 m and the carbonate spike at depth 2.5 is undermined by the presence of the red band at depth 2.35 m, which is likely the thin remnant of a buried horizon.

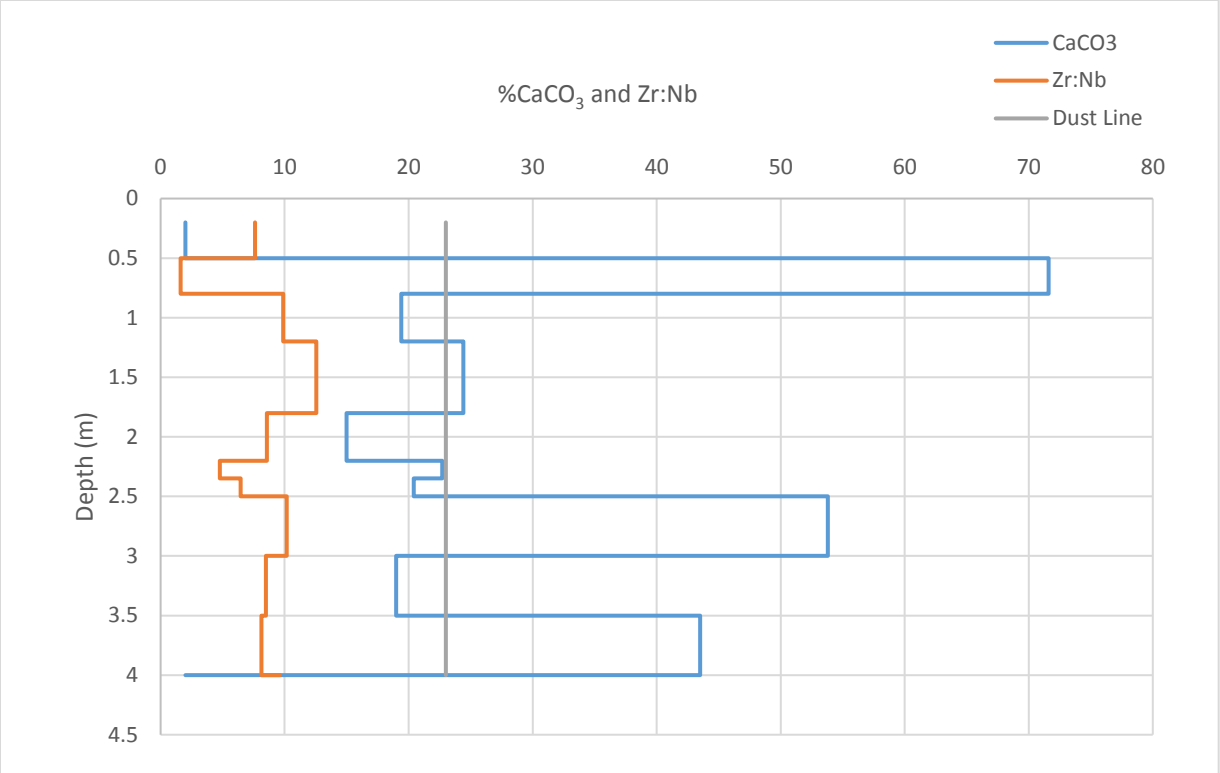

Figure 14: Zr:Nb plotted against %CaCO3 from FTIR and a Zr:Nb value for regional dust. Regional dust ration taken from (Pelletier et al. 2011). The petrocalcic, laminar cap is at 0.5 meters depth. The low value for Zr:Nb is due to the cap being comprised primarily carbonate. Some correlation in the upper portion of the profile exists between the eolian proxy and carbonate accumulation.

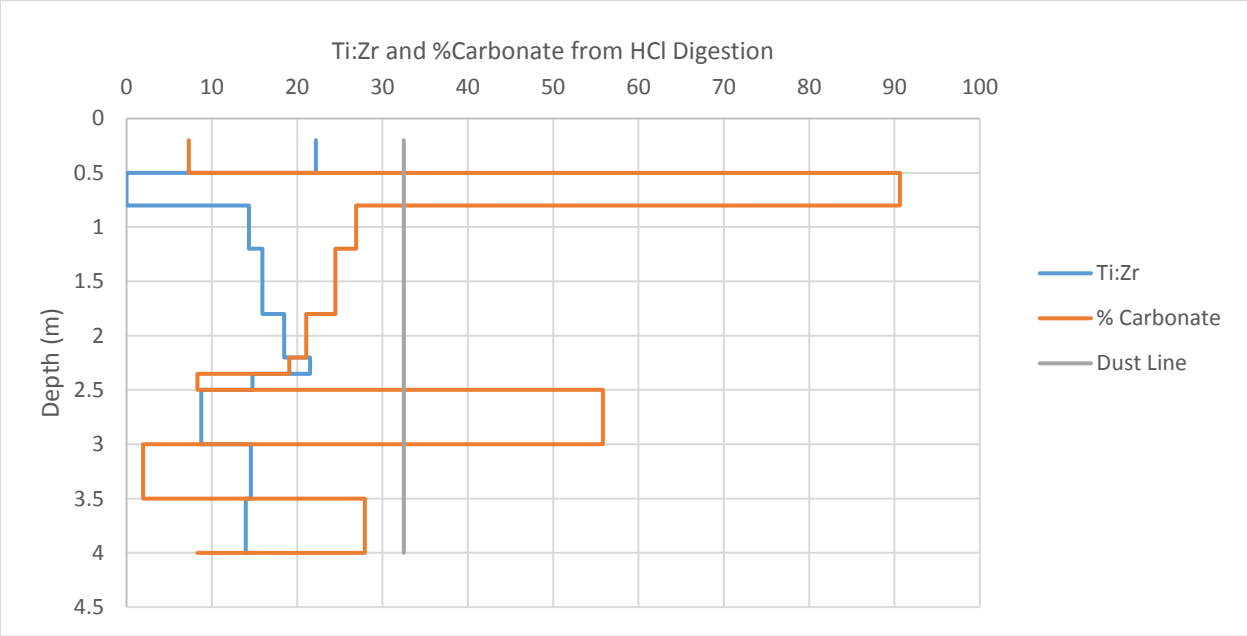

Figure 15: Ti:Zr eolian proxy plotted against carbonate accumulation value derived from HCl digestion. Correlation between the proxy and carbonate accumulation is again weak.

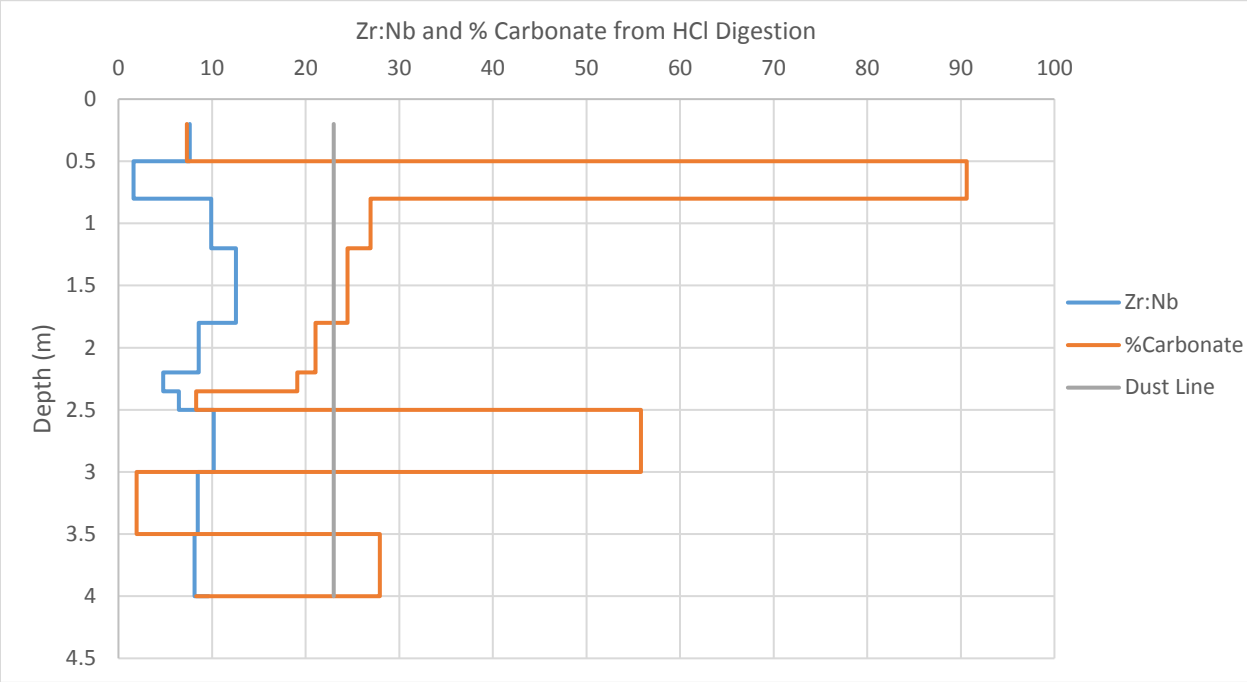

Figure 16: Zr:Nb eolian proxy plotted against carbonate concentration derived from the HCl digestion method. Again, some correlation between the proxy and the carbonate accumulation exists in the upper portion of the profile.

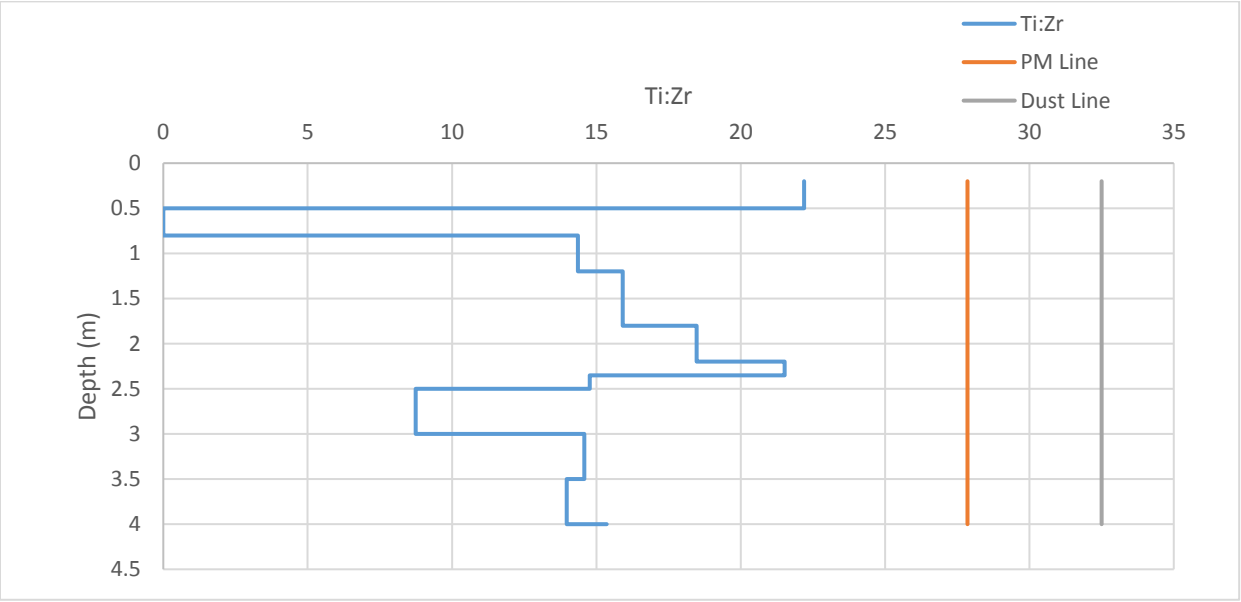

Figure 17: Sediment Ti:Zr plotted against the Ti:Zr value obtained for the parent material. Parent material values were taken from the coarse fraction of the basal gravel, sample 2410. The general shape of the titanium change throughout the profile (fig) is quite similar to the change seen in the Ti:Zr proxy suggesting that the change in the proxy is driven primarily by the change in titanium. Where titanium rises above the PM line, external contribution of titanium is the cause. Where it fluctuates below the PM line has to be due to removal of titanium or the deposition of materials containing less titanium.

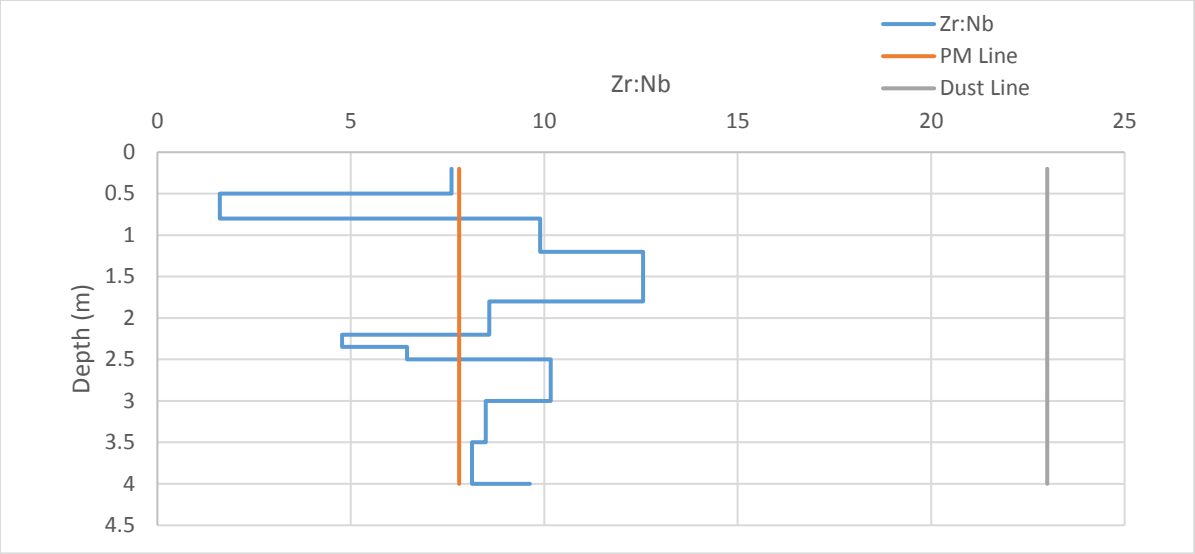

Figure 18: Zr:Nb eolian proxy plotted against the parent material Zr:Nb value and the dust value for this proxy. Zr:Nb hovers close to the PM line throughout the profile.

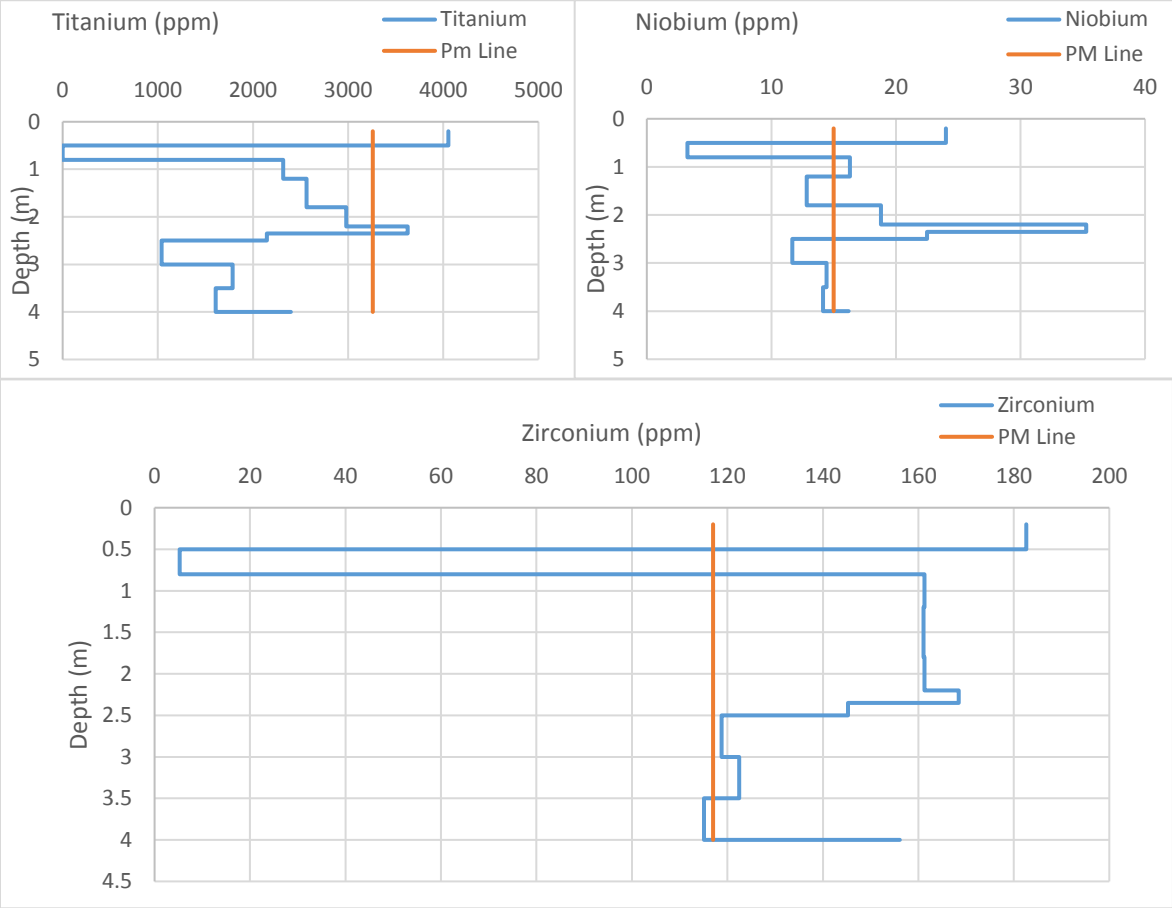

Figure 19: Immobile element ppm throughout the profile plotted against their respective parent material values in ppm. Niobium and Zirconium show quantitatively small shifts compared to titanium, which shifts as high as approximately 2500 ppm.

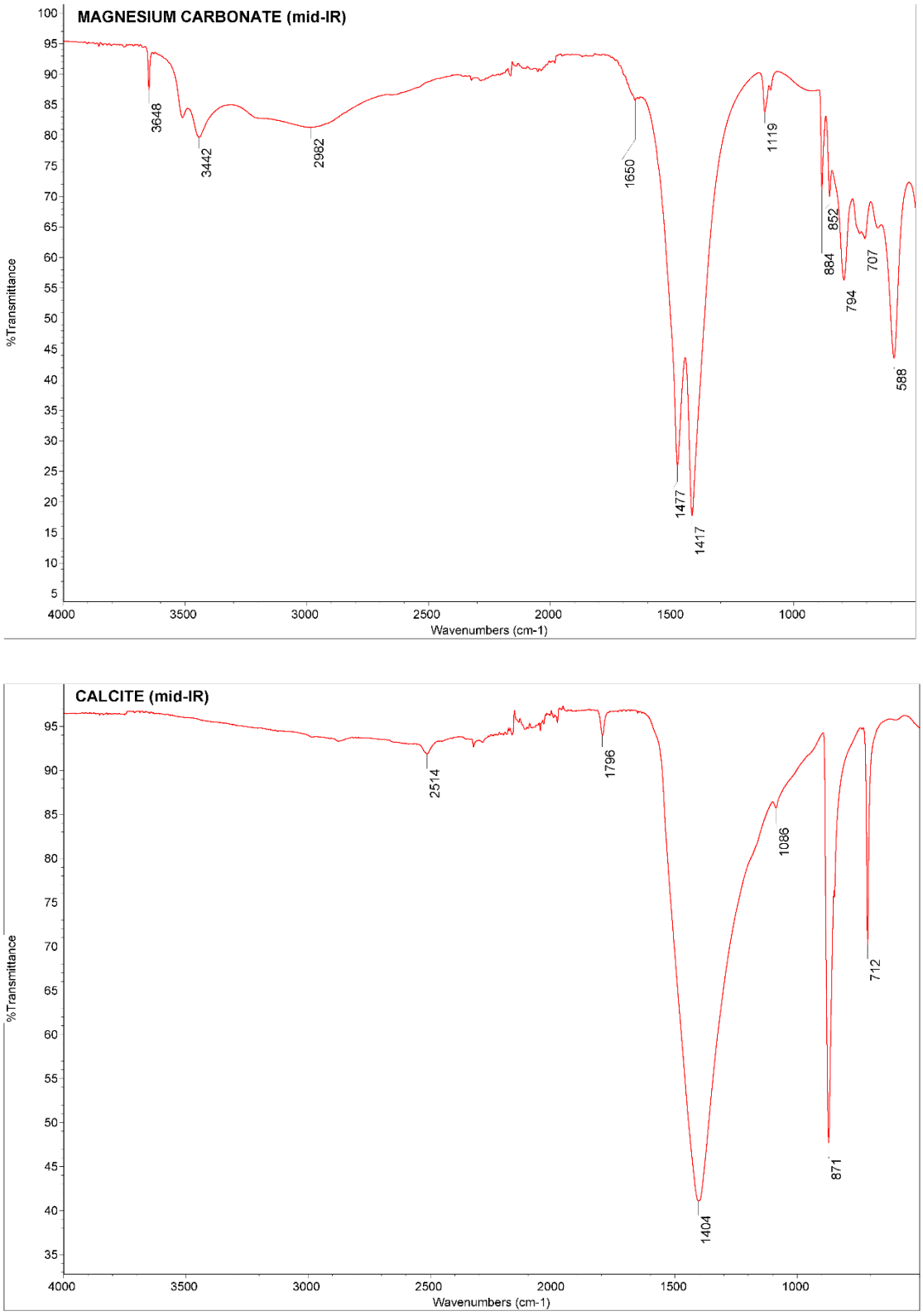

Figure 20: Comparison of Near IR spectra of CaCO3 and MgCO3 from ATR-FTIR.

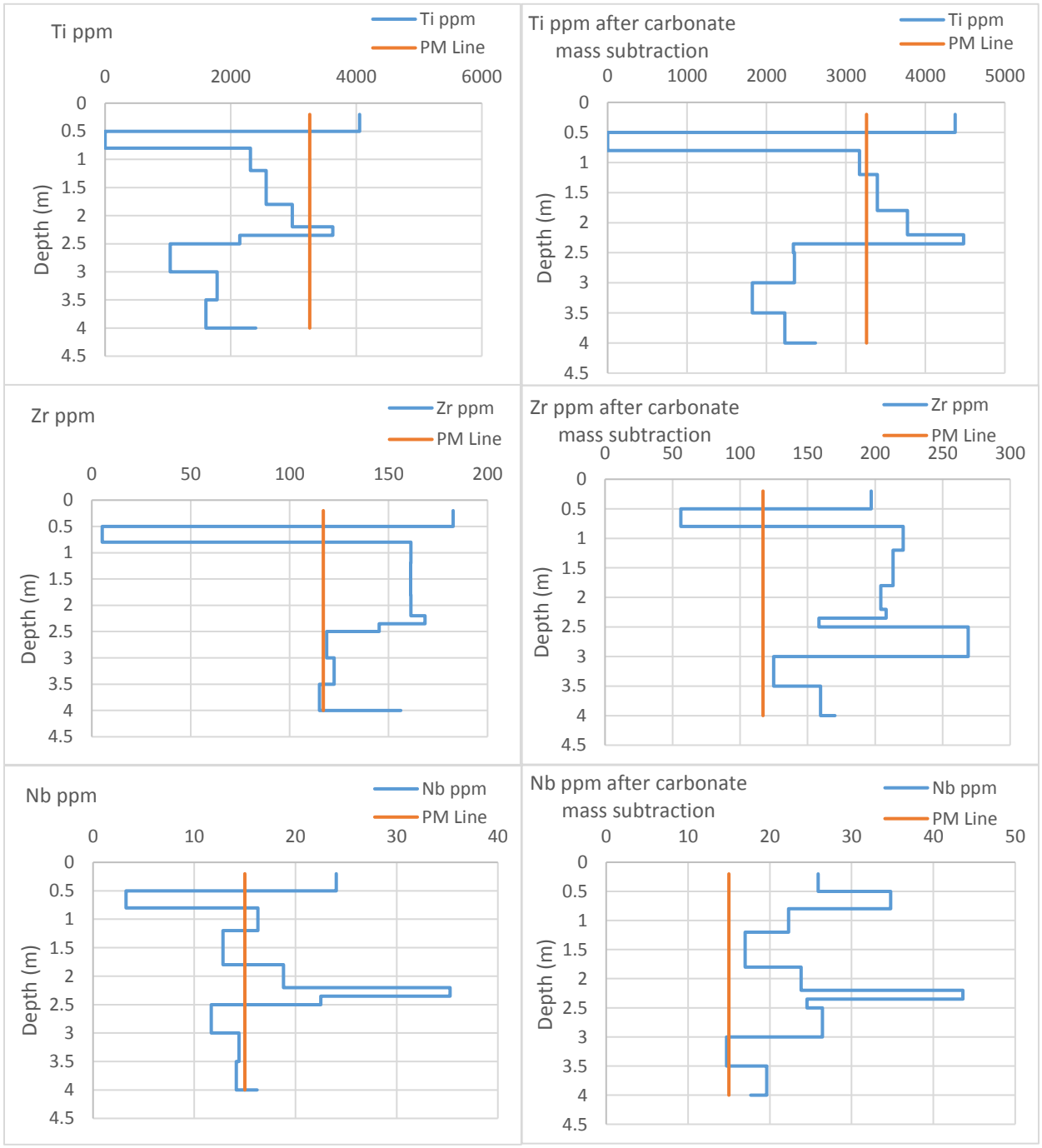

Figure 21: Immobile element plots comparing concentrations where carbonate mass is included and where carbonate mass has been subtracted. Subtraction of the carbonate mass resulted increases in all elements that drove Nb ad Zr above their parent material lines, suggesting an external source for these elements.

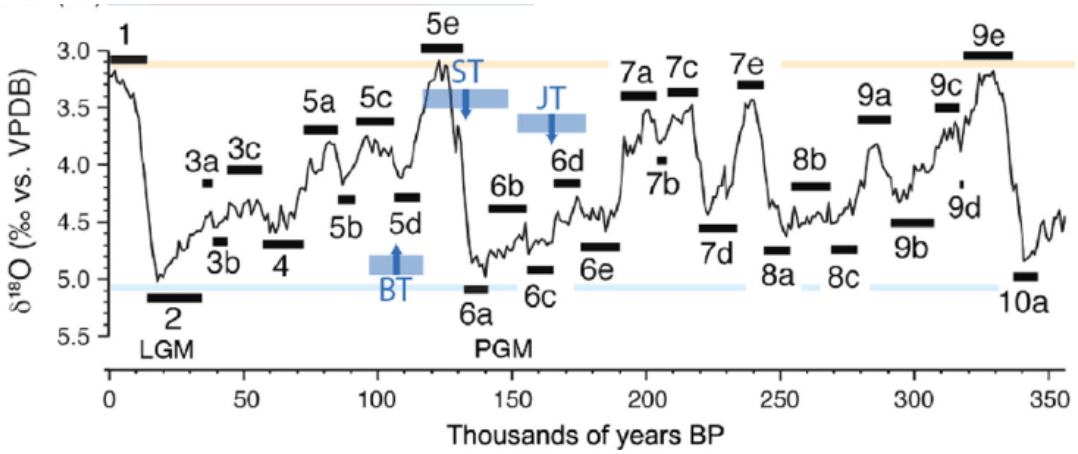

Figure 22: Marine Isotope record taken from Pickering et al. (2017), modified from Railsback et al (2015)

Horizon	Depth (cm)	Moist color	Texture	%Clay	%RF	Struct.	Cons.	pH	Roots	CaCO3	Clay Films
A	0-10	7.5 YR 3/2	Sandy clay loam	30	30Gr 15St	1M Platy IF SBK	SH	6.6	1M, 3F, 3VF	1	-
AB	10-18	5 YR 3/2	Silty clay	55	50Cb	IM SBK	HA	7.4	1M, 3F, 3VF	0	-
Bt	18-35	2.5 YR 2/4	Clay	60	40Gr	2C SBK 2M SBK	FI	8.1	1M, 2F, 2VF	1	3C, P, PF
Bkkm	35-39	-	-	-	-		VS	8.3		4	

Table 1: Field Characteristics of uppermost soil at the Saddlebrooke site. Classification: shallow, clayey, skeletal, mixed, superactive, thermic Ustalfic Petrocalcid. Diagnostic horizons: ochric 0-10cm, argillic 18-25cm, petrocalcic 35-38cm. "RF" indicates rock fragments.

		XRF Elemental ppm			FTIR		HCL	Iron mg/g soil	
Sample	Depth (m)	Nb	Ti	Zr	Reflectance	%CaCO3	%Carbonate	Dith	AmOx
2400	0.2	24.02	4053.09	182.61	98	2	7.33	21.9	0.031
2401	0.5	3.26	0	5.26	39.157	71.6	90.63	na	na
2402	0.8	16.3	2316.43	161.29	60.987	19.4	26.93	2.026	0.015
2403	1.2	12.83	2563.5	161.07	57.176	24.4	24.48	1.523	0.169
2404	1.8	18.81	2979.25	161.31	65.283	15	21.05	2.214	0.161
2405	2.2	35.28	3625.32	168.43	58.377	22.7	19.09	1.712	0.391
2406	2.35	22.5	2145.23	145.23	60.173	20.4	8.31	2.403	0.819
2407	2.5	11.68	1038.34	118.76	43.95	53.8	55.84	1.272	0
2408	3	14.43	1785.36	122.45	61.343	19	1.94	1.774	0.05
2409	3.5	14.15	1607.56	115.06	47.497	43.5	27.91	1.9	0
2410	4	16.21	2398.45	156.15	98	2	8.31	3.284	1.067

Table 2: Raw data from analysis methods

REFERENCES

Andes E and Ebihara M. (1982). *Solar-system Abundances of the Elements.* Geochimica et Cosmochimica Acta. Vol: 46. Pg: 2363-2380.

Art HW, Bormann FH, Voight GK, and Woodwell GM. (1974). *Barrier island forest ecosystem: role of meteorologic nutrient inputs.* Science. Vol: 184. Is: 4132. Pg: 60-62.

Artobelli N, Postberg F. Fiege K, Trieloff M, Kimura H. Sterken VJ, Hsu HW, Hillier J, Khawaja N, Morogas-Klostermeyer G, Blum J, Burton M, Srama R, Kempf S and Gruen E. (2016). *Flux and Composition of Interstellar Dust at Saturn from Cassini's Cosmic, Dust Analyzer.* Science. Vol: 352. Is: 6283. Pg: 312-318.

Blakey, RC. (2012). *Paleogeography and Paleotectonics of Southwestern North America.*
Colorado Plateau Geosystems, DVD Flagstaff, Arizona.

Boettinger JL and Southard RJ. (1991). *Silica and carbonate sources for Aridisols on a granitic pediment, Western Mojave Desert.* Soil Science Society of America Journal. Vol: 55. Pg: 1057–1067.

Brockheim JG. (2014). *Calcic and Petrocalcic Horizons*. Soil Geography of the USA: A Diagnostic Horizon Approach. Pg: 109-122.

Buol SW, Southard RJ, Graham RC, and McDaniel PA. (2003.) *Soil Genesis and Classification.* Iowa State Press. Ed: 5th Pg: 211.

Condie KC and DeMalas JP. (1985). *The Pinal Schist: An Early Proterozoic Quartz Wacke association in Southeastern Arizona.* Precambrian Research. No: 27. Pg: 337-356.

Chadwick OA and Davis JO. (1990). *Soil-forming interval caused by eolian sedimentation in the Lahontan basin, Northwestern Nevada.* Geoderma Vol: 18. Pg: 243–246.

Damon PE, Livingston DE, and Erickons RC. (1962) *New K-AR Dates for the Precambrian of Pinal, Gila, Yavapai and Coconino Counties, Arizona.* New Mexico Geological Society; 13th Field Conference. Pg: 56,57.

Davis GH, Constenius KN, Dickinson WR, Rodriguez EP, and Cox LJ. (2004). *Fault and fault-rock characteristics associated with Cenozoic extension and core-complex evolution in the Catalina-Rincon region, southeastern Arizona.* GSA Bulletin. No: 116(1-2). Pg: 128-141.

Dorale JA, Edwards RL, Alexander EC, Shen CC, Richards DA and Cheng H. (2004). *Uranium-Series Dating of Speleothems: Current Techniques, Limits, & Applications*. In: Sasowsky I.D., Mylroie J. (eds) *Studies of Cave Sediments*. Springer, Boston, MA Pg: 177-197.

Dunbar NW and Hervic RL. (1992). *Petrogenesis and Volatile Stratigraphy of the Bishop Tuff: Evidence from melt Inclusion Analysis*. Journal of Geophysical Research. Vol: 97. No: B-11, Pg: 15129-15150.

Ehlers J, Gibbard PL and Hughes PD. (2018). *Chapter 4-Quaternary Glaciations and Geochronology.* In, *Past Glacial Environments 2nd Ed.* Elsevier Ltd. Pg: 77-101.

Enzel Y, Wells SG, and Lancaster N. (2003). *Late Pleistocene lakes along the Mohave River, Southeast California.* Geologic Society of America special paper. No: 238. Pg: 61-77.

Feng Q, Endo KN, and Chang, G. (2000) *Soil Carbon in Desertified Land in Relation to Site Characteristics.* Geoderma. No: 106. Pg: 21-43.

Figueora-Cisterna J, Bagur-Gonzalez MG, Morales-Ruano S, Carrillo-Rosua J, and Martin-Peinado F. (2011). *The use of a combined portable X-ray fluorescence and multivariate statistical methods to assess a validated macroscopic rock samples classification in an ore exploration survey*. Talanta. Vol: 85. Is: 5. Pg: 2307-2315.

Fischer A, Shepard C, and Rasmussen C. (2017). *Geochemical Differences in Petrocalcic and Calcic Horizons due to Soil Parent Material in Southeastern Arizona.* GSA Poster.

Fletcher KE, Heizler MT, Karlstrom KE, Timmons JM, Crossley LJ, and Bloch JD. (2004). *Provenance and Geochronology of Metaproterozoic Sedimentary Rocks from Across the Southwest United States Revealed by 40 Ar/39Ar Dating of Detrital Muscovites.* Geological Society of America, Abstracts with Programs. Vol: 36. No: 5. Pg: 405.

Fornash KF, Patchett JP, Gehrels GE, and Spencer JE. (2013). *Evolution of Granitoids in the Catalina Metamorphic Core Complex, Southeastern Arizona: U–Pb, Nd, and Hf Isotopic Constraints.* Contributions to Mineralogy and Petrology. Vol: 165. Is: 6. Pg: 1295-1310.

Gifford RM. (1994). *The Global Carbon Cycle: a Viewpoint on the Missing Sink*. Australian Journal of Plant Physiology. Vol: 21(1). Pg: 1–15.

Goren Y, Mommsen H, and Klinger J. (2011). *Non-destructive Provenance Study of Cuneiform Tablets Using Portable X-Ray Fluorescence (pXRF)*. Journal of Archaeological Science. Vol: 38. Is: 3. Pg: 684-696.

Heindyl LA and McClaymons NE. (1964). *Younger Pre-Cambrian Formations and the Bolsa (?) Quartzite of Cambrian Age, Papago Indian Reservation.* Arizona. Unites States Geological Survey Professional Paper. No: 501-C. Pg: C43-C49.

Ibarra DE, Egger AE, Weaver KL, Harris CR, and Maher K. (2014). *Rise and Fall of Late Pleistocene Pluvial Lakes in Response to Reduced Evaporation and Precipitation: Evidence from Lake*

Surprise, California. Geological Society of America Bulletin. No: 126 (11-12). Pg: 1387-1415.

Izett GA, Obradovich JD and Mehnert HH. (1988). *The Bishop Ash Bed (Middle Pleistocene) and Some Older (Pliocene and Pleistocene) Chemically and Mineralogically Similar Ash Beds in California, Nevada and Utah.* U.S. Geological Survey Bulletin 1675.

Junge CE and Werby RT. (1958) *The Concentration of Chloride, Sodium, Potassium, Calcium and Sulfate in Rainwater Over the United States.* Journal of Meteorology. Vol: 15. No: 5. Pg: 417-425.

Jungers MC and Heimsath AM. (2015). *Post-tectonic Landscape Evolution of a Coupled Basin and Range: Pinaleno Mountains and Safford Basin, Southeastern Arizona.* Geological Society of America Bulletin. Vol: 128. No: ¾. Pg: 469-486.

Jungers MC and Heimsath AM. (2018). *Transverse Canyon Incision and Sedimentary Basin Excavation Driven by Drainage Integration, Aravaipa Creek, AZ, USA.* Earth Surface Processes and Landforms. Vol: 44. Is: 5. Pg: 1077-1090.

Labaj MA and Pratt BR. (2016). *Depositional Dynamics in a Mixed Carbonate–Siliciclastic System: Middle–Upper Cambrian Abrigo Formation, Southeastern Arizona, U.S.A. Journal of Sedimentary Research.* No: 86 (1). Pg: 11–37.

Lattman L. (1973). *Calcium Carbonate Cementation of Alluvial Fans in Southern Nevada*. GSA Bulletin 84 (9). Pg: 3013-3028.

LaViolette PA. (1984). *Evidence for High Cosmic Dust Concentrations in Late Pleistocene Polar Ice (20,000–14,000 years B.P.).* Meteoritics and Planetary Science. Vol: 20. Is: 3. Pg: 545-558.

Liu Z and Zhao J. (2000). *Contribution of Carbonate Rock Weathering to the Atmospheric CO_2 Sink.* Environmental Geology. Vol: 39. Is: 9. Pg: 1053–1058.

Livingston DE. (1969). *Geochronology of Older Precambrian Rocks in Gila County, Arizona*. Unpubl. Ph.D. Dissertation, Univ. Arizona, Tucson, Pg: 224.

Loste E, Wilson RM, Seshadri R. and Meldrum FC. (2003).*The role of Magnesium in Stabilising Amorphous Calcium Carbonate and Controlling Calcite Morphologies.* Journal of Crystal Growth. Vol: 254. Is: 1-2. Pg: 206-218.

Ma L, Chabaux F, Pelt E, Granet M, Sak PB, Gaillardet J, Lebedeva M, and Brantley SL. (2012). *The Effect of Curvature on Weathering Rind Formation: Evidence from Uranium-series Isotopes in Basaltic Andesite Weathering Clasts in Guadeloupe.* Geochimica et Cosmochimica Acta. Vol: 80. Pg: 92-107.

Machette MN, (1985). *Calcic Soils of the Southwestern United States*. In: Weide DL (ed) *Soils and Quaternary Geology of the Southwestern United States*. Geological Society of America, Special paper. Vol: 203. Pg: 1–21.

Marion GM. (1989). *Correlation Between Long-Term Pedogenic $CaCO_3$ Formation Rate and Modern Precipitation in Deserts of the American Southwest*. Quaternary Research. Vol: 32. Is: 3. Pg: 291-295.

Maybeck M. (1987). *Global Chemical Weathering of Surficial Rocks Estimated from River Dissolved Loads.* American Journal of Science. Vol: 287. Pg: 401-428.

McFadden LD and Tinsley JC. (1985). *Rate and Depth of Pedogenic-Carbonate Accumulation in Soils: Formulation and Testing of a Compartment Model*. Soils and Quaternary Geology of the Southwestern United States, Geological Society of America Special Paper. Is. 203. Pg: 23-41.

McFadden LD. (1981). *Quaternary evolution of the Canada del Oro Valley, Southeastern Arizona*. Arizona Geological Society Digest. Vol: 13. Pg: 13-19.

McKeague JA and Day JH. (1966). *Dithionite and Oxalate-Extractable Fe and Al as Aids in Differentiated Various Classes of Soils.* Canadian Journal of Soil Science. Vol: 46. Pg: 13-22.

McKeague JA, Brydon JE and Miles NM. (1971). *Differentiation of Forms of Extractable Iron and Aluminum in Soils*. Soil Science Society of America Journal. Vol: 35. No: 1. Pg: 33-38.

Mehra OP and Jackson ML. (1960). *Iron Oxide Removal from Soils and Clays by a Dithionate-citrate System Buffered with Sodium*

Bicarbonate. Clays and Clay Minerals: Proceedings from the Seventh National Conference. Vol: 5. Pg: 317-327.

Menges CM and McFadden LD. (1981). *Evidence for Latest Miocene to Pliocene Transition from Basin-range Tectonic to Post-tectonic Landscape Evolution in Southeastern Arizona.* Arizona Geological Society Digest. Vol: 13. Pg: 151-160.

Meszaros E. (1966). *On the Origin and Composition of Atmospheric Calcium Compounds*. Tellus. Vol: 18. Is: 2-3. Pg: 262-265.

Mi N, Wang S, Liu J, Yu G, Zhang W, and Jobaggy E. (2008). *Soil Inorganic Storage Pattern in China.* Global Change Biology. Vol: 4. Is: 10. Pg: 2380-2387.

Middleton LT and Trujillo AP. (1984). *Sedimentology ad Depositional Setting of the Upper Paleozoic Scanlon Conglomerate, Central Arizona.* Canadian Society of Petroleum Geologists, Sedimentology of Gravels and Conglomerates. Mem: 10. Pg: 189-201.

Monger HC, Daughtery LA, Lindermann WC, and Liddell CM. (1991). *Microbial Precipitation of Pedogenic Calcite.* Geology. No: 19. Pg: 997-1000.

Morrison RB. (1991). *Quaternary Geology of the Southern Basin and Range Province.* In Morrison RB ed. *Quaternary Nonglacial Geology; Conterminous U.S.: Boulder, Colorado*. Geological Society of America, The Geology of North America, Vol: K-2. Pg: 353-371.

Nash DJ. (2011). *Desert Crusts and Rock Coatings.* In Thomas DSG. *Arid Zone Geomorphology: Process, Form and Change in Drylands, 3rd Ed.* John Wiley & Sons Ltd. Pg: 131-180.

NRCS. (2019). *Aridisols Map.* United States Department of Agriculture. http://www.nrcs.usda.gov/wps/portal/nrcs/detail/soils/survey/class/maps/?cid=nrcs142p2_053595

Pelletier JD, McGuire LA, Ash, JL, Engelder TM, Hill LE, Leroy KW, Orem CA, Rosenthal WS, Trees MA, Rasmussen C, and Chorover J. (2011). *Calibration and Testing of Upland Hillslope Models in a Dated Landscape: Banco Bonito, New Mexico*. Journal of Geophysical Research. Vol: 116. Is: F04004.

Pickering J, Goodbred S, Beam J, Ayers J, Covey A, Rajapara H, and Singhvi A. (2017). *Terrace formation in the Upper Bengal Basin Since the Middle Pleistocene: Brahmaputra Fan Delta Construction During Multiple Highstands.* Basin Research. Pg: 1-18

Rabenhorst MC, Wilding LP and West LT. (1984). *Identification of Pedogenic Carbonates Using Stable Carbon Isotope and Microfabric Analyses*. Soil Science Society of America Journal. Vol: 48. Pg: 125–132.

Rabenhorst MC and Wilding LP. (1986a). *Pedogenesis on the Edwards Plateau. Texas: I. Nature and Continuity of parent material*. Soil Science Society of America Journal. Vol: 50. Is: 3. Pg: 678–687

Rabenhorst MC and Wilding LP. (1986b). *Pedogenesis on the Edwards Plateau. Texas III. New Model for the Formation of Petrocalcic Horizons*. Soil Science Society of America Journal. Vol: 50. Is: 3. Pg: 693–699.

Rasmussen C. (2006). *Distribution of Soil Organic and Inorganic Carbon Pools by Biome and Soil Taxa in Arizona.* Soil Science Society of America Journal. Vol: 70. Is: 1. Pg: 256-265.

Reheis MC, Budahn JR, Lamothe PJ, and Reynolds, RL. (2009). *Compositions of Modern Dust and Surface Sediments in the Desert Southwest, United States.* Journal of Geophysical Research. Vol: 114. FO1028

Retallack G. (2005). *Pedogenic Carbonate Proxies for Amount and Seasonality of Precipitation in Paleosols.* Geology. Vol: 33. Is: 4. Pg: 333-336.

Richard SM, Reynolds SJ, Spencer JE and Pearthree PA. (2000). *Geologic Map of Arizona.* Arizona Geological Survey Map # 35.

Royer DL. (1999). *Depth to Pedogenic Carbonate Horizon as a Paleoprecipitation Indicator?* Geology. Vol: 27. Is: 12. Pg: 1123-1126.

Schindler DW. (1999). *The Mysterious Missing Sink.* Nature; London. Vol: 398, Is: 6723, Pg: 105-107.

Schmitt AD and Stille P. (2005). *The Source of Calcium in Wet Atmospheric Deposits: Ca-Sr Isotope Evidence.* Geochimica et Cosmochimica Acta. Vol: 69. Is: 14. Pg: 3463-3468.

Shaetzl R and Anderson S. (2005). *Soils: Genesis and Morphology.* Cambridge University Press. Pg: 768.

Shankar N and Achyuthan H. (2007). *Genesis of Calcic and Petrocalcic Horizons from Coimbatore, Tamil Nadu: Micromorphology and Geochemical Studies.* Quaternary International. Vol: 175. Is: 1. Pg: 140-154.

Sheperd C. (2018). *Understanding Quaternary Soil Formation Using a Synthesis of Soil Chronosequences.* University of Arizona, Soil Water and Environmental Science. Doctoral Dissertation.

Schulz KJ, Piatak NM, and Papp JF. (2017). *Niobium and Tantalum.* US Geological Survey Professional Paper # 1802-M

Shride AF. (1967). *Younger Precambrian Geology in Southern Arizona.* Geological Survey Professional paper. No: 566.

Silver L. (1978). *Precambrian Formations and Precambrian History in Cochise County, Southeastern Arizona*. N.M. Geological Society Guidebook. 29th Field Conference. Pg: 157--163.

Sobecki TM and Wilding LP. (1983). *Formation of Calcic and Argillic Horizons in Selected Soils of the Texas Coast Prairie.* Soil Science Society of America Journal. Vol: 47. Is: 4. Pg: 707-715.

Soil Survey Staff. (2010). *Keys to Soil Taxonomy, 11th Edition.* USDA Natural Resources Conservation Service, Washington, DC. Pg: 644.

Spencer JE, Richard SM, and Ferguson CA. (2000). *Compilation Geologic Map of the Oracle 7.5 Quadrangle, Pinal and Pima Counties, Arizona.* Arizona Geological Survey Open File Report 00-05.

Stroud water Research Center. (2018). *Model my Watershed.* Wikiwatershed. https://wikiwatershed.org/model/

Tatarko, J. (1980). *Effect of Calcium Carbonate on the Distribution of Creosote bush (Larrea tridentate (DC.) Coville) in West Texas and Southern New Mexico.* Texas Tech University. Thesis.

Turk JK, Chadwick OA, and Graham RC. (2012). *Pedogenic Processes.* In Huang PM, Li Yuncong and Sumner ME. *Handbook of Soil Sciences: Properties and Processes, 2nd Ed.* CRC Press. Pg: 30-1 to 30-29.

Vahur S, Teearu A, Peets P, Joosu L. and Leito I. (2016). *ATR-FT-IR Spectral Collection of Conservation Materials in the Extended Region of 4000 – 80 cm^{-1}.* Analytical and Bioanalytical Chemistry. Vol: 408. Is: 13. Pg: 3373-3379.

Van der Hoven SJ and Quade J. (2002). *Tracing Spatial and Temporal Variations in the Sources of Calcium in Pedogenic Carbonates in Semiarid Environment*. Geoderma Vol: 108. Pg: 259–276.

Walker JD, Geissman JW, Bowring SA and Babcock LE. (2013). *The Geologic Society of America Geologic Timescale.* Geological Society of America Bulletin, March/April. Vol: 125. No: 3-4. Pg: 259-272.

Weir CE and Lippincott ER. (1961). *Infrared Studies of Aragonite, Calcite and Vaterite Type Structures in the Borates, Carbonates and Nitrates*. Journal of Research of the National Bureau of Standards-A. Physics and Chemistry. Vol: 65A. No: 3. Pg: 173-183.

Whipkey CE, Capo RC, Chadwick OA, Stewart BW. (2000). *The Importance of Sea Spray to the Cation Budget of a Coastal Hawaiian Soil: a Strontium Isotope Approach.* Chemical Geology. Vol: 168. Is: 1-2. Pg: 37-48.

Wickham S and Oxburgh R. (1985) *Continental Rifts as Settings for Regional Metamorphism.* Nature. No: 318. Pg: 330-333.